The auxin-regulated CrRLK1L kinase *ERULUS* controls cell wall composition during root hair tip growth

Sébastjen Schoenaers[a,§], Daria Balcerowicz[a,§], Gordon Breen[b], Kristine Hill[c,1], Malgorzata Zdanio[a], Grégory Mouille[d], Tara J. Holman[c], Jaesung Oh[c,2], Michael H. Wilson[c,3], Natalia Nikonorova[e,f], Lam Dai Vu[e,f,g,h], Ive De Smet[e,f], Ranjan Swarup[c], Winnok H. De Vos[i,j], Isabel Pintelon[i], Dirk Adriaensen[i], Claire Grierson[b], Malcolm J. Bennett[c], Kris Vissenberg[a,k,4,*]

[a] Integrated Molecular Plant Physiology Research, Biology Department, University of Antwerp, Groenenborgerlaan 171, 2020 Antwerpen, Belgium

[b] School of Biological Sciences, University of Bristol, BS8 1UG, United Kingdom

[c] Centre for Plant Integrative Biology, School of Biosciences, Sutton Bonington Campus, University of Nottingham, Loughborough LE12 5RD, United Kingdom

[d] Institut Jean-Pierre Bourgin UMR1318 INRA/AgroParisTech, ERL3559 CNRS, Saclay Plant Sciences, route de St Cyr, 78026 Versailles, France.

[e] Department of Plant Biotechnology and Bioinformatics, Ghent University, 9052 Ghent, Belgium

[f] Center for Plant Systems Biology, VIB, 9052 Ghent, Belgium

[g] VIB-UGent Center for Medical Biotechnology, VIB, Ghent, Belgium,

[h] Department of Biochemistry, Ghent University, Ghent, Belgium

[i] Laboratory of Cell Biology and Histology, Department of Veterinary Sciences, University of Antwerp, Universiteitsplein 1, 2610 Wilrijk, Belgium

[j] Cell Systems Group, Dept. Molecular Biotechnology, University of Ghent, Coupure Links 653, 9000 Ghent, Belgium

[k] Plant Biochemistry & Biotechnology Lab, Department of Agriculture, Technological Educational Institute of Crete, Stavromenos PC 71410, Heraklion, Crete, Greece

[1] Present address: Center for Plant Molecular Biology – ZMBP, Developmental Genetics, University of Tübingen, Auf der Morgenstelle 32D - 72076 Tübingen, Germany

[2] Present address: Plasma Technology Research Center, National Fusion Research Institute, 37 Dongjangsan-Ro, Gunsan-Si, Jeollabuk-Do 54004, Republic of Korea

[3] Present address: Centre for Plant Sciences, University of Leeds, Leeds LS2 9JT, United Kingdom

[4] Lead Contact: Kris Vissenberg, Integrated Molecular Plant Physiology Research, Biology Department, University of Antwerp, Groenenborgerlaan 171, 2020 Antwerpen, Belgium, kris.vissenberg@uantwerpen.be, phone: +32-32653410

[§] These authors contributed equally to this work.

* Correspondence: Kris Vissenberg, Integrated Molecular Plant Physiology Research, Biology Department, University of Antwerp, Groenenborgerlaan 171, 2020 Antwerpen, Belgium, kris.vissenberg@uantwerpen.be, phone: +32-32653410

Sébastjen Schoenaers: Sebastjen.Schoenaers@uantwerpen.be, Daria Balcerowicz: daria.balcerowicz@uantwerpen.be, Gordon Breen: gordonjlbreen@gmail.com, Kristine Hill: kristine.hill@uni-tuebingen.de, Malgorzata Zdanio: malgorzata.zdanio@uantwerpen.be, Grégory Mouille: gregory.mouille@versailles.inra.fr, Tara J. Holman: tara_lawrence@hotmail.co.uk, Jaesung Oh: ohjs@nfri.re.kr, Michael H. Wilson: m.h.wilson@leeds.ac.uk, Natalia Nikonorova: natalia.nikonorova@ugent.be, Lam Dai Vu: lam.vu@psb.vib-ugent.be, Ive De Smet: ivsme@psb.vib-ugent.be, Ranjan Swarup: ranjan.swarup@nottingham.ac.uk, Winnok De Vos: winnok.devos@uantwerpen.be, Isabel Pintelon: Isabel.pintelon@uantwerpen.be, Dirk Adriaensen: dirk.adriaensen@uantwerpen.be, Claire Grierson: Claire.grierson@bristol.ac.uk, Malcolm J. Bennett: malcolm.bennett@nottingham.ac.uk, Kris Vissenberg: kris.vissenberg@uantwerpen.be

Keywords: auxin, kinase, root hair, cell wall, pectin, tip growth, *Arabidopsis*, CrRLK1L, AUXIN RESPONSE FACTOR, FERONIA, AHA2

Summary

Root hairs facilitate a plant's ability to acquire soil anchorage and nutrients. Root hair growth is regulated by the plant hormone auxin and dependent on localized synthesis, secretion and modification of the root hair tip cell wall. However, the exact well wall regulators in root hairs controlled by auxin have yet to be determined. In this study, we describe the characterization of ERULUS (ERU), an auxin-induced *Arabidopsis* receptor-like kinase whose expression is directly regulated by ARF7 and ARF19 transcription factors. ERU belongs to the *Catharanthus roseus* RECEPTOR-LIKE KINASE 1-LIKE (CrRLK1L) subfamily of putative cell wall sensor proteins. Imaging of a fluorescent fusion protein revealed that ERU is localized to the apical root hair plasma membrane. ERU regulates cell wall composition in root hairs and modulates pectin dynamics through negative control of pectin methylesterase (PME) activity. Mutant *eru* (-/-) root hairs accumulate de-esterified homogalacturonan and exhibit aberrant pectin Ca^{2+} binding site oscillations and increased PME activity. Up to 80% of the *eru* root hair phenotype is rescued by pharmacological supplementation with a PME inhibiting catechin extract. *ERU* transcription is altered in specific cell wall-related root hair mutants, suggesting it is a target for feedback regulation. Loss of *ERU* alters the phosphorylation status of FERONIA and H^+-ATPases 1/2, regulators of apoplastic pH. Furthermore, H^+-ATPases 1/2 and ERU are differentially phosphorylated in response to auxin. We conclude that *ERULUS* is a key auxin-controlled regulator of cell wall composition and pectin dynamics during root hair tip growth.

Introduction

Root hairs (RH) elongate via a tip-based growth mechanism [1]. Several studies have shown that tip growth occurs in an oscillatory manner and is accompanied by oscillations of cytoplasmic Ca^{2+} levels [2], extracellular reactive oxygen species (ROS) and pH [3]. The plant hormone auxin is a key component of RH tip growth since several auxin response mutants exhibit RH phenotypes [4], whilst auxin supplementation promotes RH elongation [5] and the expression of the core RH transcription factor RSL4 changes in response to exogenous IAA application [6]. Auxin Response Factors (ARFs) control transcription of auxin-responsive genes [7]. However, despite the reported role of auxin in controlling RH elongation, besides *RSL4* none of the tip growth related genes have been identified as direct targets of ARFs [8]. Factors that control RH tip growth ultimately direct the delivery of CW and plasma membrane material to the expanding tip and control the modification (loosening/tightening) of the CW at the tip apex [9]. Interestingly, the transcription of a number of CW related genes was altered in loss-of-function and overexpression lines of the auxin-regulated RH TF RSL4 [6]. However, no direct link between auxin signaling and RH CW composition or dynamics has been reported to date.

RH growth is facilitated by the coordinated synthesis, secretion, recycling and remodelling of CW material. The formation of an organized and dynamic matrix of cellulose, hemicellulose and pectin polymers is required to control plasticity at the tip and provide structural support in the subapical stalk. Failure to do so often results in mutants with aberrant RH morphology [10–13]. Loss of *FERONIA,* a member of the *Catharanthus roseus* RLK1-like (CrRLK1L) subfamily of putative CW sensing proteins, was also shown to drastically impair RH morphogenesis [14], whilst the RLK-VII member called MARIS regulates RH growth downstream of the CrRLK1L signaling pathway [15]. Despite these advances, the structural and regulatory complexity of the RH CW have proven difficult to dissect.

Here, we report on the characterization of *ERULUS*, a RH-specific member of the CrRLK1L subfamily. We show that *ERU* transcription is regulated by auxin, with its promoter being a direct target for ARF7 and ARF19 TFs. In addition, auxin treatment alters ERU phosphorylation status. We demonstrate that ERU localizes to the *Arabidopsis* apical RH plasma membrane and regulates RH growth through modulation of pectin methylation dynamics. Mutant plants lacking ERU exhibit short, bulged RHs, a higher pectin methylesterase (PME) activity and drastically altered pectin Ca^{2+} binding site oscillations. Pharmacological inhibition of PME activity rescued up to 80% of the *eru* RH phenotype. Furthermore, loss of *ERU* function results in differential phosphorylation of FERONIA (FER) and H^{+}-ATPases 1/2 (AHA1/2), regulators of apoplastic pH. In addition, AHA1/2 is differentially phosphorylated on auxin treatment. We conclude that auxin controls pectin related CW composition in growing RHs via the CrRLK1L family protein ERULUS, through a pathway that likely involves FER and AHA1/2 action.

Results

The receptor-like kinase ERU regulates tip growth in root hairs

To identify new root hair (RH) tip growth related genes, two Affymetrix ATH1 array datasets were cross-correlated. The first dataset was prepared using RNA from the root differentiation zones of wild type (WT; Col-0) plants and the *rhd2* loss-of-function mutant that fails to extend RH bulges due to the absence of a functional ROS gradient [16]. The second dataset was prepared using FACS-sorted root epidermal cells from protoplasted lines in which either every epidermal cell was a RH (*wer myb* double mutant) or a non-hair cell (*cpc try* double mutant) [17]. Data integration led to the selection of 150 genes whose expression was positively correlated with RH tip growth.

Reverse genetic screens of the candidate genes identified a T-DNA insertion in a *Catharanthus roseus* receptor-like kinase 1-like (CrRLK1L) kinase named *ERULUS (ERU),* which, as previously reported, resulted in severely aberrant RH morphology (Figure 1A)[14,18]. Genotypic analysis revealed that the T-DNA was inserted 1047 bp downstream of the start codon (Figure S1A) and resulted in a complete loss of *ERU* transcript (Figure S1B). The *erulus* (-/-) plants developed very short RHs (22.4% of the WT length, Figure 1A,B) that often bulged at the tip. RH positioning at the basal end of root epidermal cells was unaffected, and distinct trichoblast cell files were present in *eru* plants (Figure S1C). Contrary to previous findings, the short/bulged *eru* RH phenotype persisted when grown on minimal growth medium (Figure S1D,E) [18]. By insertion of the 2529 bp native promoter coupled to its coding sequence and GFP (*ERUp::ERU-GFP)* into the *eru* (-/-) mutant *Arabidopsis* background, we were able to fully complement the *eru* short RH phenotype (Figure 1A,B), demonstrating protein functionality. In addition, we no longer observed RH bulging in the complemented lines. 35S driven *ERU* overexpression (*35S::ERU)* in the *eru* or Col-0 background did not alter the final WT RH length or the RH profile (Figure 1B, Figure S1F-H).

To investigate at which stage of RH development *ERU* is involved, we constructed RH profiles and monitored single RH growth of 7-day-old WT and *eru* roots (Figure 1C,D). In WT roots, RHs elongated through tip growth at a constant growth rate until they reached maturity (600-700 µm) at a distance

of ±3 mm from the root tip (Figure 1C). *eru* RHs grew much slower, but kept doing so for the same extent of time as WT RHs. Bulge formation occurred normally in *eru* plants, but mutant RHs were unable to make the subsequent switch to fast tip growth (Figure 1D). After bulge formation, WT RHs switched to tip growth with a constant growth rate of 0.93 ± 0.05 µm min^{-1}, whereas *eru* RHs grew at 0.30 ± 0.03 µm min^{-1}. Moreover, during the expected period of fast tip growth, *eru* RHs experienced occasional growth interruption after which slower than normal growth was regained. Based on our findings, we concluded that ERU is essential to controlling tip growth in RHs.

ERU encodes a trichoblast plasma membrane localized receptor-like kinase enriched at the root hair tip

To determine the tissue-specific expression of *ERU* we constructed a transcriptional fusion of its promoter with the GFP reporter (*ERUp::GFP*). A public transcriptomics dataset indicated trichoblast specific expression [19]. Visualization of >4 independent stably transformed T_3 WT plants carrying the *ERUp::GFP* transgene revealed that *ERU* transcription is restricted to trichoblast cell files (Figure 2A), confirming the public transcriptomics data [19]. GFP was first detected in elongating epidermal cells, even before RH bulge formation. The *ERU* promoter was active throughout RH morphogenesis, then GFP signal intensity decreased gradually after RH maturation (Figure S2A). These findings were independently confirmed using GUS as an alternative reporter (Figure S2B-D).

Next, we investigated ERU subcellular localization. ERU contains a N-terminal signal peptide (M1-S27), a Malectin receptor-like domain (F28-A425) with 6 putative N-linked glycosylation sites (N81, N125, N252, N294, N359, N365), a hydrophobic transmembrane domain (I426-V446) and a C-terminal cytoplasmic domain (R447-P842) coding for a protein kinase. As such, ERU was likely to be trafficked via the secretory pathway to the plasma membrane. Bioinformatic analysis for non-redundant *A. thaliana* protein sequences with similarity to the ERU signal peptide combined with GO enrichment analysis revealed a strong overrepresentation of 'extracellular region' associated proteins (Figure S3A), amongst which included FERONIA, pectin lyase-like, pectin methylesterase inhibitor and proline rich extensin-like proteins. We identified a highly conserved hydrophobic motif (Figure S3B,C) with a presumable targeting function (N-terminal in 71 % of all cases) which was present in all identified proteins. In parallel, we transformed WT and *eru Arabidopsis* plants with a transgene containing the *ERU* coding sequence coupled to a C-terminal GFP reporter and driven by its native promoter (*ERUp::ERU-GFP)*. In all independent lines, we observed that ERU-GFP specifically localized to the future site of RH formation, the RH bulge and the very tip of tip-growing RHs (Figure 2B). High resolution spinning disk confocal microscopy revealed that ERU-GFP localized to an endomembrane compartment which accumulated at the surface of the RH bulge (Figure 2C; movie S1) or the growing RH tip (Figure 2D-F; movie S2) and to the apical plasma membrane in RH bulges (Figure 2C; movie S1) and tip-growing RHs (Figure 2D-F; movie S2). ERU protein localization at the tip seemed highly dynamic yet displayed no oscillatory behaviour (movie S3; Figure S4). Hence, ERU represents a trichoblast-specific RLK that localizes to the apical plasma membrane of RHs.

ERU is regulated by auxin via ARF7 and ARF19 transcription factors which directly bind to its promoter

The plant hormone auxin is known to positively regulate root hair growth [5]. To assess the role of ERU in auxin-mediated RH development, we transferred 5-day-old WT and *eru* seedlings to medium containing different concentrations of IAA, NAA and 2,4D. Although auxin treated *eru* (-/-) RHs were markedly longer than untreated controls (up to 63% of the WT RH length) and no longer bulged, we were unable to fully complement their RH length defect (Figure S5A-D). Importantly, *eru* RH growth velocity remained 51% lower compared to WT RHs upon 20 nM IAA supplementation (Figure S5D). Hence, ERU represents an important component of the auxin signaling pathway required to promote RH growth.

In silico analysis of the *ERU* promoter sequence identified four canonical auxin response elements (AuxREs), positioned at 462, 1454, 1999 and 2596 bp upstream of the ATG start codon, and encoded by the TGTCTC/GAGACA conserved ARFAT sequence, or single nucleotide variants thereof (e.g. TGTCAC at -462, Figure 3A). In addition, multiple core TGTC/GACA auxin response elements were also present (Figure 3A). Auxin response factors (ARFs) bind to AuxREs to regulate auxin-mediated transcription [7]. Besides others, *ARF7* and *ARF19* are both actively transcribed in growing RHs [19](Figure S5E). We quantified *ERU* transcription in response to auxin application in WT and *arf7arf19* double mutant roots. In *Col-0*, *ERU* mRNA abundance peaked 30 min after auxin application after which it rapidly decreased to reach baseline levels after 120 min (Figure 3B). In contrast, in *arf7arf19* roots *ERU* mRNA level remained very low. Hence, *ERU* transcript abundance is regulated in an ARF7/ARF19 dependent manner with expression dynamics consistent with being a primary auxin response gene.

To directly test whether ARF7 and/or ARF19 bind to the *ERU* promoter, we performed chromatin immuno-precipitation PCR (ChIP-PCR) studies. Chromatin was extracted from WT, *arf7* (-/-) and *arf19* (-/-) root cultures, after which ChIP-PCR studies were performed using ARF7 and ARF19 specific antibodies (Figure S5F). Real time PCR using primers specifically designed to amplify the regions associated with the -462 and -1454 localized ARFAT sites revealed that ARF7 (both AuxREs) and ARF19 (-462 AuxRE) directly bind to the *ERU* promoter (Figure 3C,D). Relative to *arf7* and *arf19* null mutants, *ERU* associated promoter DNA was significantly enriched in anti-ARF7 (Figure 3C) and anti-ARF19 (Figure 3D) immuno-precipitated fractions compared to the input DNA fractions (non-immuno-precipitated controls). Taken together, our results reveal *ERU* transcription is controlled by auxin and represents a direct target for at least ARF7 and ARF19 transcription factors.

ERU is phosphorylated at serine 497 in response to auxin

Protein phosphorylation is an important post-translational modification controlling protein function. Auxin is known to induce proteome-wide phosphorylation changes [20] and e.g. controls the phosphorylation status/activity of H^+-ATPase during acid-growth directed hypocotyl elongation [21]. It was previously shown that ERU function depends on its phosphorylation status [22]. To study the effect of auxin treatment on ERU phosphorylation, we checked ERU protein phosphorylation in a data set generated from *Arabidopsis* root tips in response to NAA (100 nM) treatment (unpublished results). We found that the abundance of the ERU peptide **S**NGFSSFFSNQGLGR, which corresponds to the serine 497 phosphosite (pS497), increased by a factor of 6.94 ± 2.87 (n=5) upon auxin treatment (Figure 4, Figure S6A). Since serine 497 lies within the cytoplasmic protein domain and has not been functionally annotated, it is unclear how its phosphorylation affects ERU action. Importantly however, our data illustrates a second (post-translational) means through which auxin may regulate ERU function.

ERU transcription is altered in pectin cell wall mutants

ERU belongs to the CrRLK1L family of putative CW sensing proteins. To investigate whether *ERU* transcription is altered in response to changes in RH CW composition, we quantified *ERU* transcript in 7-day-old roots of several RH CW mutants (*repressor of lrx1 1, rol1; leucine-rich repeat/extensin1, lrx1; leucine-rich repeat/extensin2, lrx2; enhancer of lrx1 7, enl7*; *procuste1*, *prc1; cellulose synthase-like d3, csld3; theseus1, the1).* ROL1, or repressor of LRX1 1, encodes a UDP-L-Rhamnose synthase that is responsible for modification of the pectic polysaccharides rhamnogalacturonan I and II [13]. The *lrx1-1* mutant phenotype, which is the result of aberrant CW architecture, is suppressed by both allelic *rol1* mutations [13]. As such, it has been suggested that LRX1 could be involved in the establishment of a functional pectin matrix [13]. LRX2 functions redundantly with LRX1, and Enhancer Of Lrx1 (ENL7) worsens the *lrx1-1* phenotype, suggesting they are functionally related [23]. *PROCUSTE1* (*PRC1), CELLULOSE SYNTHASE-LIKE D3 (CSLD3)* and *THESEUS1 (THE1)* encode a cellulose synthase (CESA6), a protein required for the synthesis of a non-cellulosic wall polysaccharide and normal cellulose and

xyloglucan organization in RH CWs, and a CW/cellulose deficiency sensor protein of the CrRLK1L family, respectively [24–26]. *ERU* transcription was 1.6-fold upregulated in the *rol1-2* null mutant, and~2-fold downregulated in the *lrx1-1*, *enl7* and *lrx2-1* mutants, but remained unaffected in *prc1-1, csld3* and *the* roots (Figure S7A). These findings suggest that some, but not all, CW perturbations alter *ERU* gene expression, indicative of feedback regulation from the CW. Notably, *ERU* transcript abundance was altered in the *rol1* and *lrx1-1* RH mutants which, in literature, have been related to pectin [13].

ERU is a regulator of cell wall metabolism in root hairs

Next, we investigated whether differences existed in the CW composition of *eru* and WT RHs using micro Fourier Transform Infrared Spectroscopy (microFT-IR). We observed significant differences in IR absorbance at several distinct wavenumbers (Figure 5A), some of which had been annotated to specific CW components [27–29]. These likely corresponded to the underrepresentation of the pectin (845-864) and xyloglucan (XYG) ring structures (922-949), and over representation of the glycosydic C-O-C linkage vibration of cellulose (1150 and 1161 doublet) in *eru* RHs (Figure 5B)[27–29].

To probe the observed changes in CW composition, we analysed cellulose, xyloglucan and pectin distribution in the CW of WT and *eru* RHs using dyes, antibodies and confocal microscopy. Direct red 23 (also known as pontamine fast scarlett) was used to visualize cellulose [30]. In WT RHs, we detected high fluorescence intensity at the tip (consistent with the site of cellulose synthesis), and lower intensity in the RH stalk (Figure S7B). In agreement with our microFT-IR data, the fluorescence intensity in the stalk of *eru* RHs was much higher compared to WT RHs (Figure S7B). Cellulose overaccumulation could be due to a higher cellulose synthase (CesA) activity or normal CesA activity in combination with slower RH growth. To discriminate between both, we deduced the CW thickness from the acquired confocal images (Figure S7C) and cross-correlated it with the observed cellulose content (Figure S7D). The width of the CW correlated significantly with the cellulose content (Rho = 0.80). The CW of *eru* RHs was twice as thick as WT RHs. We calculated the CW volume for a hypothetical 200 µm RHs cylinder (Figure S7E,F) and found that it inversely related to RH growth speed (Figure S7G). The volume of the cytosol remained unaffected (Figure S7H). Hence, overaccumulation of cellulose in *eru* is likely a secondary effect of slow RH growth.

Next, we directly determined the overall XYG content in the RH primary CW using a monoclonal antibody with specificity towards several XYG oligosaccharides. In agreement with our microFT-IR spectra, we observed that *eru* RHs accumulate 1.7-fold less XYG compared to WT RHs (Figure S7I). We also investigated pectin composition using monoclonal antibodies towards methylesterified and de-esterified HG epitopes (Figure 5). Interestingly, *eru* RHs had much lower methyl-esterified and far higher de-esterified HG levels in the RH stalk compared to WT, suggesting a higher degree of de-esterification by pectin methylesterases (PMEs). The total HG content (the sum of methyl-esterified and de-esterified HG) remained unaffected (Figure 5C). Using a coupled enzymatic approach, we quantified PME activity in root tips (containing growing RHs) of WT and *eru* roots. Consistent with our previous observations, we detected a 1.6-fold increase in PME activity in the *eru* mutant. To verify that the observed RH growth effect was related to increased PME activity we supplemented WT and *eru* plants with different concentrations of Polyphenon 60 (PP60), a catechin extract shown to inhibit PME-activity in a concentration-dependent manner by direct binding to PME or to its substrate pectin, thereby blocking PME access [31]. PP60 supplementation rescued *eru* RH length up to 80% that of WT RHs, showing that increased PME activity is a major factor contributing to the *eru* phenotype (Figure 6).

Given the apparent role of ERU in regulating pectin dynamics and the low XYG content in the *eru* RH CW, we were interested to see if a XYG/pectin compensation mechanism could exist in RHs. The existence of such a mechanism in controlling CW biomechanics has been suggested before, but has

never been illustrated in RHs [32]. Unfortunately, pectin-deficient RH mutants have not been identified to date, making it impossible to test XYG accumulation therein. However, we found that XYG deficient *xxt1/2/5* RHs contain 1.9-fold more pectin Ca^{2+} binding sites and have a thicker CW (Figure S7L-N). The latter finding suggests that XYG and pectin can assume a compensatory role to maintain CW rigidity, which could explain the CW composition observed in *eru* RHs.

To further understand how pectin dynamics were affected in *eru* RHs, we visualized the availability of pectin Ca^{2+} -binding sites (a direct consequence of de-esterification by PME-activity) via *in vivo* propidium iodide (PI) staining of growing RHs [9]. Time lapse imaging revealed a higher PI intensity (consistent with higher PME activity), but much slower oscillations in *eru* RHs (Figure 5E,F; movie S4). In WT RHs pectin Ca^{2+} binding sites oscillated at 0.018 ± 0.0009 Hz, and in 14 out of 20 RHs a secondary component at a frequency of 0.007 ± 0.002 Hz was present (Figure 5G,H), whereas in *eru* RHs, the main frequency of oscillation was drastically slower at 0.003 ± 0.0003 Hz and was characterized by an amplitude ~13-fold greater than WT RHs (Figure 5G,H). Each *eru* oscillation was marked by a sudden and steep increase in PI fluorescence, followed by a gradual decrease to original levels, whereas in WT RHs, each oscillation was characterized by a discrete rise and equal decrease in PI signal intensity (movie S4). The average apical PI signal intensity in *eru* RHs remained 3-fold higher compared to WT RHs throughout acquisition (Figure S7J) and never reached WT levels, even after maturation (Figure S7K). Taken together, our data show that ERU plays a crucial role in CW composition and pectin metabolism through regulation of PME activity.

FERONIA and H^+-ATPase 2 are differentially phosphorylated in ERU loss-off-function root tips

To identify downstream targets of the ERU kinase and gain insight in how ERU could regulate cell wall dynamics, we compared the phosphoproteome of WT and *eru* root tips (containing the root differentiation zone). We found that FERONIA (FER) and a peptide corresponding to H^+-ATPase 1 and/or 2 (AHA1/2), all of which are involved in regulating apoplastic pH [14,33], were significantly differentially phosphorylated at serine 701 (pS701; **S**FGYLDPEYFR) and serine 904 (pS904; EL**S**EIAEQAKR), respectively (Figure 7, Figure S6B,C). FER pS701 phosphopeptide abundance had decreased 3.4-fold (Figure 7A) and AHA1/2 pS904 phosphopeptide abundance had increased by a factor of 2.9 (Figure 7C) in the *eru* mutant background, whereas overall peptide abundance remained unaffected (Figure 7B,D). FER pS701 is located in the cytoplasmic kinase domain and has not yet been functionally annotated. When expressed in yeast, phosphorylation of AHA1/2 S904, a cytoplasmic phosphosite located in the C-terminal autoinhibitory regulatory domain, leads to protein activation [34]. This domain also contains the presumable FER-targeted phosphosite AHA2 S899, which has been shown to regulate AHA2 proton pumping activity [14]. As such, our data reveal that ERU might function through regulation of FER and AHA1/2 phosphorylation, which controls apoplastic pH and potentially indirectly also cell wall enzyme activity during cell elongation.

Interestingly, we found that auxin supplementation (100 nM NAA) caused a 1.6- and a 1.3-fold decrease in the abundance of the AHA1/2 G**S**YRELSEIAEQAK and AHA2 GLDIE**T**PSHYTV phosphopeptides, corresponding to previously characterized AHA2 S899 and T947 phosphosites, known to activate AHA's pumping activity (Figure S6D-I). Importantly, these NAA-addition data should be interpreted with care as this data set does not reveal cell type-specific changes in the root so that the general changes could mask potential other effects present specifically in root hairs. Nevertheless, our results demonstrate an *in planta* regulation of AHA1/2 by both auxin and ERU, further supporting that both players are embedded in the same signalling network.

Discussion

RH tip growth represents one of nature's most rapid forms of cell elongation. A hormone-driven pathway controls CW rheology at the RH tip to withstand turgor pressure, yet to provide sufficient flexibility for growth. The hormone auxin controls RH expansion [5], yet knowledge about its direct targets for regulation of cell wall dynamics have been lacking, to date. We describe the characterisation of the cell wall receptor-like kinase ERULUS, a key regulator of RH expansion. *Eru* (-/-) plants exhibit a RH growth defect (Figure 1). We report that (1) *ERU* is specifically expressed in trichoblasts, (2) ERU is a key component of auxin-driven RH growth, (3) ERU is a direct target of at least ARF7 and ARF19, (4) ERU phosphorylation is altered in response to auxin, (5) ERU localizes to the apical RH plasma membrane (PM) and (6) ERU regulates CW composition/dynamics during RH elongation, possibly through affecting FER and AHA1/2 phosphostatus and subsequently their activity. Whilst our ERU subcellular localisation results contrast with the findings of Bai et al. (2014), which can have various reasons, we demonstrate that our *ERUp*::*ERU-GFP* reporter rescued the *eru* (-/-) RH defect in *Arabidopsis t.*, providing confidence that our ERU PM localisation results are valid [18].

ERU is a member of the CrRLK1L family of putative CW sensing kinases and contains a malectin-like domain, which has been hypothesized to bind specific CW polysaccharides or glycoproteins [35]. Several CrRLK1L proteins associate with CW modification or sensing during expansion [35]. We illustrate that *ERU* has a role in controlling the CW machinery in RHs. CW turnover and modification is concentrated at the tip. We found that ERU localizes to the tip PM in growing RHs, throughout all RH developmental stages (Figure 2B-F, movie S1-3). The ERU signal peptide is likely to encode an extracellular localization signal (Figure S3), targeting the malectin-like domain to the CW where it could potentially interact with carbohydrate-containing ligands or small signaling peptides (such as RALFs interacting with FER [14,36]).

At the growing RH apex, the load bearing capacity of the CW is thought to be determined by the interconnectivity of the cellulose/XYG "grid" and the fluidity of the pectin matrix, yet empirical data to support this theory is scarce. In pollen tubes, highly methyl-esterified HG (major pectin component) is exocytotically secreted at the RH tip [37]. Subsequent de-esterification by PMEs would then generate de-esterified HG that can be degraded by pectin lyases (resulting in higher CW flexibility) or interact through egg-boxes with Ca^{2+} ions to generate a stiff crosslinked matrix [38]. The availability of pectin Ca^{2+}-binding sites was shown to oscillate at the same frequency as the RH growth velocity, implicating that PME activity may oscillate too [9]. *eru* RHs exhibit aberrant CW composition. The mutant has a thicker, cellulose-enriched CW (Figure S7B-D), and much lower amounts of XYG (Figure S7I). In addition, ERU functions as a negative regulator of PME activity (Figure 5C,D) since *eru* RHs were devoid of methyl-esterified and enriched in de-esterified HG, whilst PME-activity was higher in mutant root extracts. This finding is supported by the fact that pharmacological treatment with a PME-inhibiting catechin extract resulted in a highly substantial rescue of the *eru* phenotype (Figure 6). Moreover, HG Ca^{2+}-binding site oscillations were drastically altered in mutant RHs (Figure 5E-H, Figure S7J,K, movie S4), illustrating a continuously higher potential of the CW to bind Ca^{2+} and thus provide a highly cross-linked HG matrix. In line with previous findings, we found that a pectin/XYG compensation mechanism to control CW biomechanics might also exist in RHs, thereby explaining lower XYG abundance in the highly rigid pectin-altered *eru* CW (Figure S7L-N)[32]. Further characterization of XYG/pectin functional dependency would increase our understanding of how CW plasticity is regulated. Consistent with its role as a putative CW sensor, *ERU* transcription was altered in specific RH CW mutants, suggesting *ERU*/CW feedback regulation (Figure S7A).

The mechanism linking ERU-mediated regulation of cell wall composition and PME activity is currently unknown. In primary root cell expansion, RAPID ALKALINIZATION FACTOR (RALF)-induced apoplastic alkalinisation is mediated by the physical interaction between RALF and the CrRLK1L FER, and subsequent FER kinase-controlled phosphorylation of AHA2, regulating AHA2 pumping activity [14]. In addition, the constitutively expressed AHA1 was also found to regulate root apoplastic pH. The FER/AHA2 mechanism has been illustrated in primary root cell elongation, but not shown to regulate RH development. Importantly, we now found that the *eru* mutation results in differential phosphorylation of FER and AHA1/2, suggesting that a similar mechanism might operate in RH tips (Figure 7). PME-activity, which is strongly affected in *eru* RHs, is highly pH-dependent, and likely contributes to apical pH oscillations during RH growth since PME-mediated HG demethylesterification releases protons as a byproduct [39]. In addition, RALF4 was found to be highly co-regulated with pectin modifying enzymes [40]. Moreover, the enzymes that regulate CW XYG remodelling function at a specific pH-optimum [41]. Hence, altered extracellular pH dynamics, both by altered PME activity and AHA1/2 pumping activity could explain the diverse defects observed in the *eru* CW. It is tempting to hypothesize that ERU is part of a FER-ERU-AHA1/2 apoplastic pH-regulating mechanism that alters CW metabolism in the RH tip and that, in turn, is sensitive for CW changes (by both FER and ERU). Whether the altered phosphorylation of AHA1/2 is a direct consequence of the activity of ERU or FER or another kinase remains to be shown.

Recently, it was shown that FER-mediated control of CW pH is auxin-dependent [33]. We report that in roots AHA1/2 is differentially phosphorylated at S899 and T947 in response to auxin treatment (Figure S6F-I). More so, ERU is regulated by auxin at the transcriptional (through direct binding of ARF7 and ARF19 to its promoter) and post-translational level (through auxin-induced phosphorylation). Collectively, these data reveal that auxin is strongly embedded within the pathway(s) controlling CW composition and dynamics in RHs.

Acknowledgments

The authors would like to thank the Research Foundation–Flanders (FWO), the Interuniversity Attraction Poles Programme – Belgian State – Belgian Science Policy [IUAP VI/33], the Biotechnology and Biological Sciences Research Council (BBSRC) and the University of Antwerp (TTBOF/29267) for funding. M.H.W., T.J.H., J.O., K.H., R.S. and M.J.B. acknowledge the support of the Biotechnology and Biological Sciences Research Council (BBSRC) and Engineering and Physical Sciences Research Council (EPSRC) funding to the Centre for Plant Integrative Biology (CPIB) BB/D019613/1; K.H. acknowledges BBSRC Professonial Research Fellowship funding to M.J.B., grant BB/G023972/1; and M.J.B. acknowledges the Royal Society-Wolfson Merit Award. G.B. was supported by the BBSRC Strategic Studentship BS/S/H/2005/12044, awarded to C.G.. Contributions of C.G. were funded by BBSRC Grant G19475 and the Royal Society of London Research Grant 'Arabidopsis Root Hair Functional Genomics. J.O. acknowledges the R & D programme of "Plasma Advanced Technology for Agriculture and Food (Plasma Farming)" through the National Fusion Research Institute of Korea (NFRI) funded by the Government funds. We thank Brigitte van de Cotte for assisting with (phospho)proteomics sample preparation. L.D.V. is the recipient of a VIB International Ph.D. program fellowship. The UltraVIEW VoX spinning disk confocal microscope was purchased with support of the Hercules Foundation (Hercules Type 1: AUHA 09/001).

Author contributions

K.V. conceived the project; S.S., D.B., G.B., C.G. identified and phenotyped the mutant; S.S., D.B., W.D.V. performed microscopy. I.P. and D.A. provided microscopy access. S.S.; D.B. and M.Z. performed cloning and gene expression studies; S.S. performed cell wall analysis and immuno-localizations; G.M.

provided FT-IR access; T.J.H., J.O., M.H.W., R.S. performed the auxin micro-array analysis; K.H. performed ChIP-experiments; N.N. and L.D.V. performed (phospho)proteomics; S.S., D.B. and K.H. performed qPCR; S.S. performed bio-informatics and statistics; S.S., D.B., G.M., M.H.W., I.D.S., K.H., R.S., R.B., M.J.B., C.G. and K.V. analysed and interpreted data; S.S., D.B., M.J.B. and K.V. wrote the paper.

Declaration of Interests

The authors declare no competing interests.

References

1. Schoenaers, S., Balcerowicz, D., and Vissenberg, K. (2017). Molecular mechanisms regulating root hair tip growth: a comparison with pollen tubes. In Pollen Tip Growth: From Biophysical Aspects to Systems Biology, G. Obermeyer, J. Feijo, ed. (Springer), pp. 167–243.

2. Monshausen, G.B., Messerli, M. A., and Gilroy, S. (2008). Imaging of the Yellow Cameleon 3.6 indicator reveals that elevations in cytosolic Ca^{2+} follow oscillating increases in growth in root hairs of *Arabidopsis*. Plant Physiol. *147*, 1690–1698.

3. Monshausen, G.B., Bibikova, T.N., Messerli, M. A., Shi, C., and Gilroy, S. (2007). Oscillations in extracellular pH and reactive oxygen species modulate tip growth of *Arabidopsis* root hairs. Proc. Natl. Acad. Sci. U. S. A. *104*, 20996–1001.

4. Balcerowicz, D., Schoenaers, S., and Vissenberg, K. (2015). Cell Fate Determination and the Switch from Diffuse Growth to Planar Polarity in *Arabidopsis* Root Epidermal Cells. Front. Plant Sci. *6*, 1–13.

5. Lee, R.D.-W., and Cho, H.-T. (2013). Auxin, the organizer of the hormonal/environmental signals for root hair growth. Front. Plant Sci. *4*, 448.

6. Yi, K., Menand, B., Bell, E., and Dolan, L. (2010). A basic helix-loop-helix transcription factor controls cell growth and size in root hairs. Nat. Genet. *42*, 264–267.

7. Tiwari, S.B., Hagen, G., and Guilfoyle, T. (2003). The Roles of Auxin Response Factor Domains in Auxin-Responsive Transcription. Plant Cell *15*, 533–543.

8. Mangano, S., Denita-Juarez, S.P., Choi, H.-S., Marzol, E., Hwang, Y., Ranocha, P., Velasquez, S.M., Borassi, C., Barberini, M.L., Aptekmann, A.A., *et al.* (2017). Molecular link between auxin and ROS-mediated polar growth. Proc. Natl. Acad. Sci. *114*, 5289–5294.

9. Rounds, C.M., Lubeck, E., Hepler, P.K., and Winship, L.J. (2011). Propidium iodide competes with Ca^{2+} to label pectin in pollen tubes and *Arabidopsis* root hairs. Plant Physiol. *157*, 175–187.

10. Park, S., Szumlanski, A.L., Gu, F., Guo, F., and Nielsen, E. (2011). A role for CSLD3 during cell-wall synthesis in apical plasma membranes of tip-growing root-hair cells. Nat. Cell Biol. *13*, 973–980.

11. Pena, M.J., Kong, Y., York, W.S., and O'Neill, M.A. (2012). A Galacturonic Acid-Containing Xyloglucan Is Involved in *Arabidopsis* Root Hair Tip Growth. Plant Cell *24*, 4511–4524.

12. Velasquez, S.M., Ricardi, M.M., Dorosz, J.G., Fernandez, P. V, Nadra, A.D., Pol-Fachin, L., Egelund, J., Gille, S., Harholt, J., Ciancia, M., *et al.* (2011). O-glycosylated cell wall proteins are essential in root hair growth. Science *332*, 1401–1403.

13. Diet, A., Link, B., Seifert, G.J., Schellenberg, B., Wagner, U., Pauly, M., Reiter, W., and Ringli, C. (2006). The *Arabidopsis* Root Hair Cell Wall Formation Mutant *lrx1* Is Suppressed by Mutations in the *RHM1* Gene Encoding a UDP- L -Rhamnose Synthase. Plant Cell *18*, 1630–1641.

14. Haruta, M., Sabat, G., Stecker, K., Minkoff, B.B., and Sussman, M.R. (2014). A peptide hormone and its receptor protein kinase regulate plant cell expansion. Science *343*, 408–411.

15. Boisson-Dernier, A., Franck, C.M., Lituiev, D.S., and Grossniklaus, U. (2015). Receptor-like cytoplasmic kinase MARIS functions downstream of CrRLK1L-dependent signaling during tip growth. Proc. Natl. Acad. Sci. *112*, 12211-12216.

16. Jones, M. A., Raymond, M.J., and Smirnoff, N. (2006). Analysis of the root-hair morphogenesis transcriptome reveals the molecular identity of six genes with roles in root-hair development in *Arabidopsis*. Plant J. *45*, 83–100.

17. Dinneny, J.R., Long, T. A., Wang, J.Y., Jung, J.W., Mace, D., Pointer, S., Barron, C., Brady, S.M., Schiefelbein, J., and Benfey, P.N. (2008). Cell identity mediates the response of *Arabidopsis* roots to abiotic stress. Science *320*, 942–945.

18. Bai, L., Ma, X., Zhang, G., Song, S., Zhou, Y., Gao, L., Miao, Y., and Song, C.-P. (2014). A Receptor-Like Kinase Mediates Ammonium Homeostasis and Is Important for the Polar Growth of Root Hairs in *Arabidopsis*. Plant Cell *26*, 1497–1511.

19. Brady, S.M., Orlando, D.A., Lee, J.-Y., Wang, J.Y., Koch, J., Dinneny, J.R., Mace, D., Ohler, U., and Benfey, P.N. (2007). A High-Resolution Root Spatiotemporal Map Reveals Dominant Expression Patterns. Science *318*, 801–806.

20. Zhang, H., Zhou, H., Berke, L., Heck, A.J.R., Mohammed, S., Scheres, B., and Menke, F.L.H. (2013). Quantitative Phosphoproteomics after Auxin-stimulated Lateral Root Induction Identifies an SNX1 Protein Phosphorylation Site Required for Growth. Mol. Cell. Proteomics *12*, 1158–1169.

21. Takahashi, K., Hayashi, K., and Kinoshita, T. (2012). Auxin activates the plasma membrane H^+-ATPase by phosphorylation during hypocotyl elongation in *Arabidopsis*. Plant Physiol. *159*, 632–641.

22. Zhou, Y., Zhang, L., Wu, Z., Dai, M., Li, L., Bai, L., and Song, C. (2017). Biological function analysis of the phosphorylation sites for *Arabidopsis* CAP1. Sci. Bull. *62*, 761–763.

23. Diet, A., Brunner, S., and Ringli, C. (2004). The *enl* mutants enhance the *lrx1* root hair mutant phenotype of *Arabidopsis thaliana*. Plant Cell Physiol. *45*, 734–741.

24. Singh, S.K., Fischer, U., Singh, M., Grebe, M., and Marchant, A. (2008). Insight into the early steps of root hair formation revealed by the *procusteI* cellulose synthase mutant of *Arabidopsis thaliana*. BMC Plant Biol. *8*, 1–12.

25. Wang, X., Cnops, G., Vanderhaeghen, R., De Block, S., Van Montagu, M., and Van Lijsebettens, M. (2001). *AtCSLD3*, a cellulose synthase-like gene important for root hair growth in *Arabidopsis*. Plant Physiol. *126*, 575–586.

26. Hématy, K., Sado, P.-E., Van Tuinen, A., Rochange, S., Desnos, T., Balzergue, S., Pelletier, S., Renou, J.-P., and Höfte, H. (2007). A receptor-like kinase mediates the response of *Arabidopsis* cells to the inhibition of cellulose synthesis. Curr. Biol. *17*, 922–931.

27. Kacuráková, M., Capek, P., Sasinková, V., Wellner, N., and Ebringerová, A. (2000). FT-IR study of plant cell wall model compounds: Pectic polysaccharides and hemicelluloses. Carbohydr. Polym. *43*, 195–203.

28. Séné, C.F.B., McCann, M.C., Wilson, R.H., and Crinter, R. (1994). Fourier-Transform Raman and Fourier-Transform lnfrared Spectroscopy; An investigation of five higher plant cell walls and their components. Plant Physiol. *106*, 1623–1631.

29. Yang, J., and Yen, H. (2002). Early salt stress effects on the changes in chemical composition in leaves of ice plant and *Arabidopsis*. A Fourier transform infrared spectroscopy study. Plant Physiol. *130*, 1032–1042.

30. Anderson, C.T., Carroll, A., Akhmetova, L., and Somerville, C. (2010). Real-time imaging of cellulose reorientation during cell wall expansion in *Arabidopsis* roots. Plant Physiol. *152*, 787–796.

31. Lewis, K.C., Selzer, T., Shahar, C., Udi, Y., Tworowski, D., and Sagi, I. (2008). Inhibition of pectin methyl esterase activity by green tea catechins. Phytochemistry *69*, 2586–2592.

32. Park, Y.B., and Cosgrove, D.J. (2012). Changes in Cell Wall Biomechanical Properties in the Xyloglucan-Deficient *xxt1*/*xxt2* Mutant of *Arabidopsis*. Plant Physiol. *158*, 465–475.

33. Barbez, E., Dünser, K., Gaidora, A., Lendl, T., and Busch, W. (2017). Auxin steers root cell expansion via apoplastic pH regulation in *Arabidopsis thaliana*. Proc. Natl. Acad. Sci. *114*, E4884-E4893.

34. Fuglsang, A.T., Kristensen, A., Cuin, T. A., Schulze, W.X., Persson, J., Thuesen, K.H., Ytting, C.K., Oehlenschlaeger, C.B., Mahmood, K., Sondergaard, T.E., *et al.* (2014). Receptor kinase-mediated control of primary active proton pumping at the plasma membrane. Plant J. *80*, 951–964.

35. Nissen, K.S., Willats, W.G.T., and Malinovsky, F.G. (2016). Understanding CrRLK1L Function: Cell Walls and Growth Control. Trends Plant Sci. *21*, 516-527.

36. Stegmann, M., Monaghan, J., Smakowska-Luzan, E., Rovenich, H., Lehner, A., Holton, N., Belkhadir, Y., and Zipfel, C. (2017). The receptor kinase FER is a RALF-regulated scaffold controlling plant immune signaling. Science *355*, 287–289.

37. Bosch, M., and Hepler, P.K. (2005). Pectin Methylesterases and Pectin Dynamics in Pollen Tubes. Plant Cell Online *17*, 3219–3226.

38. Cabrera, J.C., Boland, A., Messiaen, J., Cambier, P., and Van Cutsem, P. (2008). Egg box conformation of oligogalacturonides: The time-dependent stabilization of the elicitor-active conformation increases its biological activity. Glycobiology *18*, 473–482.

39. Sénéchal, F., Wattier, C., Rustérucci, C., and Pelloux, J. (2014). Homogalacturonan-modifying enzymes: Structure, expression, and roles in plants. J. Exp. Bot. *65*, 5125–5160.

40. Wolf, S., and Höfte, H. (2014). Growth Control: A Saga of Cell Walls, ROS, and Peptide Receptors. Plant Cell *26*, 1848–1856.

41. Maris, A., Kaewthai, N., Eklöf, J.M., Miller, J.G., Brumer, H., Fry, S.C., Verbelen, J.P., and Vissenberg, K. (2011). Differences in enzymic properties of five recombinant xyloglucan endotransglucosylase/hydrolase (XTH) proteins of *Arabidopsis thaliana*. J. Exp. Bot. *62*, 261–271.

42. Clough, S.J., and Bent, A. F. (1998). Floral dip: a simplified method for *Agrobacterium*-mediated transformation of *Arabidopsis thaliana*. Plant J. *16*, 735–743.

43. Bowler, C., Benvenuto, G., Laflamme, P., Molino, F., Probst, A.V., Tariq, M., and Paszkowski, J. (2004). Chromatin techniques for plant cells. Plant J. *39*, 776–789.

44. Lavenus, J., Goh, T., Guyomarc'h, S., Hill, K., Lucas, M., Voss, U., Kenobi, K., Wilson, M.H., Farcot, E., Hagen, G., *et al.* (2015). Inference of the *Arabidopsis* lateral root gene regulatory network suggests a bifurcation mechanism that defines primordia flanking and central zones. Plant Cell *27*, 1368–1388.

45. Cho, H., Ryu, H., Rho, S., Hill, K., Smith, S., Audenaert, D., Park, J., Han, S., Beeckman, T., Bennett, M.J., *et al.* (2014). A secreted peptide acts on BIN2-mediated phosphorylation of ARFs to potentiate auxin response during lateral root development. Nat. Cell Biol. *16*, 66–76.

46. Grsic-Rausch, S., and Rausch, T. (2004). A coupled spectrophotometric enzyme assay for the determination of pectin methylesterase activity and its inhibition by proteinaceous inhibitors. Anal. Biochem. *333*, 14–18.

47. Bradford, M.M. (1976). A rapid and sensitive method for the quantitation of microgram quantities of protein utilizing the principle of protein-dye binding. Anal. Biochem. *72*, 248–254.

48. Vu, L.D., Stes, E., Van Bel, M., Nelissen, H., Maddelein, D., Inzé, D., Coppens, F., Martens, L., Gevaert, K., and De Smet, I. (2016). Up-to-Date Workflow for Plant (Phospho)proteomics Identifies Differential Drought-Responsive Phosphorylation Events in Maize Leaves. J. Proteome Res. *15*, 4304–4317.

49. Winter, D., Vinegar, B., Nahal, H., Ammar, R., Wilson, G., and Provart, N. (2007). An "electronic fluorescent pictograph" browser for exploring and analyzing large-scale biological data sets. PLoS One *2*, e718.

50. R Core team (2013). R: A Language and Environment for Statistical Computing. Available at: http://www.r-project.org.

Main-text figure legends

Figure 1. *eru* RH phenotype and growth characteristics. (A) Representative roots of 7d old WT, *eru,* WT x *35S::ERU* and *eru x ERUp::ERU-GFP* seedlings, and close-ups of RHs showing the typical short/bulged phenotype. (Scale bars: overview root, 500 µm; close-ups, 200 µm). (B) Graph showing the average final RH length of WT and *ERU* knockout, overexpression and complementation lines, relative (%) to the WT (n>10). (C) RH profile constructed from 7d old WT and *eru* seedlings (n=5). The average RH length was determined for very young RHs (1.15 mm from the root tip) until fully mature RHs (5.9 mm from the root tip). (D) growth dynamics of individual WT and *eru* RHs, showing consecutive frames of growing RHs that were followed for 1h (scale bar, 20 µm), the average growth curve and growth speed (left), and a stunted growth curve for a single representative *eru* RH (right). Arrows indicate growth pauses. RH growth dynamics were followed starting from the bulge phase and throughout the tip growth phase. Error bars represent SE. Significance codes p-value: 0.05 '*' 0.01 '**' 0.001 '***' 0.

See also Figure S1.

Figure 2. *ERULUS* tissue-specific transcription and ERULUS subcellular localization. (A) Confocal images of 7d old WT x *ERUp::GFP* showing that the *ERU* promoter activity is restricted to RH cell files only, throughout RH morphogenesis (scale bar: left, 500 µm; top right and middle, 100 µm; bottom, 25 µm). Grey-scale spinning-disc images of WT x *ERUp::ERU-GFP* showing ERU-GFP localization to (B) the future site of bulge formation, the bulge apex and the very tip of tip-growing RHs (scale bar, 20 µm), (C) vesicles and the apex during bulge formation (scale, 5 µm), (D) vesicles and the apical plasma membrane during RH tip growth (scale bar, 10 µm). (E) sequential subapical (left) to apical (right) mediolateral sections of the RH depicted in (D). (F) Frontal maximal projection of the tip from the RH depicted in (D).

See also Figure S2-4 and movie S1-3.

Figure 3. *ERU* is a target of auxin signaling. (A) The 3 kb promoter region upstream of the *ERU* start codon, showing four ARFAT (TGTCTC) sequences, for which two were assayed by qPCR after anti-ARF7 and anti-ARF19 ChIP (green markings). (B) *ERU* transcription time series after application of 1 µM NAA, in WT and the *arf7 arf19* double mutant (n=3). (C) ChIP-qPCR data showing that ARF7 binds directly to both ARFAT sequences in the *ERU* promoter (n=3). (D) ChIP-qPCR data showing ARF19 binds directly to the -475 to -353 ARFAT sequence of the *ERU* promoter (n=3). Error bars represent SE. Significance codes p-value: 0.05 '*' 0.01 '**' <0.001 '***'.

See also Figure S5.

Figure 4. ERU is differentially phosphorylated at serine 497 in response to auxin. Abundance of the ERU phosphopeptide corresponding to serine 497 in mock (black dots) and auxin supplemented (grey dots) root samples. Inset: average serine 497 ERU phosphopeptide abundance (n = 5). Error bars represent SE. Significance codes p-value: 0.05 '*'.

See also Figure S6.

Figure 5. ERU regulates pectin cell wall dynamics. (A) microFT-IR statistical output showing for which wavenumbers the t-value crosses the threshold of significance (orange lines; $\alpha = 0.05$, df= 106). Negative values represent lower IR absorbance in *eru* vs. WT RHs. Positive values represent higher IR absorbance in *eru* vs. WT RH. (B) Table showing wavenumbers at which the IR absorbance differs

significantly between *eru* (n=46) and WT (n=72) RHs, and their corresponding annotation [27–29]. For each wavenumber, absorbance values were tested for normality and statistics were performed accordingly. (C) Average intensity plot and confocal images of methyl-esterified (n=6) and de-esterified homogalacturonan (n=6; HG) in RHs (scale, 10 µm) and (D) pectin methylesterase activity at pH 7.5 (n=3). (E) Representative oscillograms of pectin Ca^{2+} binding site oscillations in growing WT and *eru* RHs and (F) representative kymographs. (G) Fourier spectra showing the main frequency of oscillation for a representative WT and *eru* RH (arrows indicate main oscillation frequencies) and (H) plot showing the average amplitude and frequency of the main fourier peaks for WT (n=22) and *eru* (n=13) RHs. Error bars represent SE. Significance codes p-value: 0.05 '*' 0.01 '**' <0.001 '***'.

See also Figure S7 and movie S4.

Figure 6. The *eru* phenotype is partially rescued by pharmacological inhibition of PME-activity. (A) final RH length of WT and *eru* RHs in the presence of different polyphenon 60 (pp60) concentrations. (B) representative images of WT and *eru* roots 2 days after pp60 supplementation (scale, 500 µm). Error bars represent SE. Significance codes p-value: 0.05 '*' 0.01 '**' <0.001 '***'.

Figure 7. The *eru* (-/-) mutation affects FERONIA and H^+-ATPase 1/2 phosphorylation status. (A) FER pS701 abundance normalized to the FER protein abundance. (B) FER peptide abundance resulting from proteome analysis. (C) AHA1/2 pS904 abundance normalized to the AHA protein abundance. (D) AHA2 and AHA1 peptide abundance resulting from proteome analysis. Dots represent abundance values in individual WT (black) and *eru* (orange) root tip samples. Bar plots represent the mean of those values. Error bars represent SE. Significance codes p-value: 0.05 '*' 0.01 '**' <0.001 '***'.

STAR Methods

KEY RESOURCES TABLE

CONTACT FOR REAGENT AND RESOURCE SHARING

Further information and requests for resources and reagents shoul be directed to and will be fulfilled by the Lead Contact, Kris Vissenberg (kris.vissenberg@uantwerpen.be).

EXPERIMENTAL MODEL AND SUBJECT DETAILS

Growth conditions

Seeds were surface sterilized prior sowing. For phenotyping and microscopy, seeds were plated on RH growth medium (3 mM KNO_3, 2 mM $Ca(NO_3)_2.4H_2O$, 0.5 mM $MgSO_4.7H_2O$, 1mM $NH_4H_2PO_4$, 1 mg ml^{-1} thiamine, 0.5 mg ml^{-1} pyridoxine-HCl, 0.5 mg ml^{-1} nicotinic acid, 0.56 mM myo-inositol, 2.3 mM MES, 25 µM KCl, 17.5 µM H_3BO_3, 1 µM $MnSO_4.H_2O$, 1 µM $ZnSO_4.7H_2O$, 0.25 µM $CuSO_4.5H_2O$, 0.25 µM $(NH_4)_6MoO_{24}.4H_2O$ and 25 µM Fe-Na EDTA) containing 0.8% phytagel and 1% sucrose at pH 5.7 or minimal medium (0.1 mM KCl, 0.1 mM $CaCl_2$, 1 mM NaCl, 1% w/v sucrose, 2% w/v agarose, pH 6). If applicable, the medium was supplemented with the indicated hormone or polyphenon 60 concentrations. For selection of transformants, seeds were sown on 1/2 Murashige and Skoog (MS) medium with vitamins (Duchefa, Netherlands), supplemented with 50 µg l^{-1} kanamycin, 25 µg l^{-1} hygromycin, 25 µg l^{-1} rifampicin and 50 µg l^{-1} gentamycin. Seeds were stratified for 2-3 days at 4°C in the dark before incubation in a growth chamber with 16 h light/8 h dark conditions, at 22°C. For ChIP-qPCR, plants were grown in 100 ml liquid media (3.2 g l^{-1} Gamborg's B5 basal salt, 1 g l^{-1} MES hydrate, 20 g l^{-1} sucrose, 1 ml l^{-1} Gamborg's B5 vitamin mix 1000X concentrated, pH 5.8) with gentle shaking in the dark for several weeks. For realtime-PCR analysis of *ERU* transcription in WT and *arf7arf19* roots, seeds were grown for 7 days in continuous light on 1/2 MS medium (1% sucrose) before being transferred to medium containing 1 µM NAA or an equivalent volume of DMSO (control). Roots were harvested 0.5, 1, 2, 4 or 6h after transferring. For phosphoproteome analysis of auxin-treated seedlings, *Arabidopsis thaliana* (ecotype Col-0) seedlings were grown vertically on ½ MS medium (0.8% agar, 1 % sucrose) containing 100 nM 1-naphthaleneacetic acid (NAA) or DMSO as a control at 22 °C and under continuous light conditions. At 11 days after germination, 1 cm root tips were harvested in 5 biological replicates.

Plant material

Arabidopsis thaliana ecotype Columbia-0 (Col-0; N1092) and mutant *eru* (SALK_083442C), *rol1-2* (CS16373), *lrx1-1* (CS16370), *lrx2-1* (CS16371), *the1-4* (SAIL_683_H03; kindly donated by Prof. Lenhard), *prc1-1* (CS297), *enl7* (CS25258), *arf7* (N24607), *arf19* (N24617), *arf7arf19* (N24629) and *xxt1/2/5* (N67828) seeds were obtained from the Nottingham *Arabidopsis* Stock Centre (ABRC) or kindly donated. Plants homozygous for the *eru* T-DNA insert were selected by PCR using T-DNA and gene-specific primers (Table S1).

METHOD DETAILS

Phenotyping

Images were collected using a Nikon AZ100 multizoom macroscope for determination of the RH length, and construction of a RH profile. RH length was measured using FIJI. For constructing a RH profile, the length of individual RHs and their distance to the root tip were measured. RH lengths were classified in 0.25 mm (normal medium) or 0.05 mm (auxin supplementation) intervals depending of their distance to the root tip, and averaged within each interval. Five independent roots were analysed. RH growth time-lapse movies were acquired using a Zeiss Axioplan microscope with a Zeiss Achroplan

100x (na 1.25) oil immersion Ph3 objective. *Eru* and Col-0 seedlings were grown on solid RH medium and gently overlaid by a cover glass. Images were collected for approx. 1 hour with a framerate of 20 s. The RH length gain was measured for each frame in FIJI for > 5 RHs.

semi-quantitative RT-PCR and real-time PCR

Total RNA was isolated from 6-day-old WT, *eru*, *rol1-2*, *lrx1-1*, *lrx2-1*, *the1-4*, *prc1-1* and *enl7* roots (PureLink®Plant RNA kit, Life Technologies), 7-day-old WT and *arf7arf19* roots, or 7-day-old roots of 6 independent WT x *35S::ERU* lines (TRIzol reagent) and DNase treated (RQ1 RNase-Free DNase, Promega). cDNA was reverse transcribed from 500 ng (CW mutants and *35S::ERU* lines) or 100 ng (*arf7arf19* mutant) of RNA using oligo(dT)20 primers. For genotyping by semi-quantitative RT-PCR *ERU, ACT2* and *EF1α* cDNA was amplified for 35 cycles (primers: table S1). For real-time PCR, taqman assays (CW mutants and *35S::ERU* lines) specific to *ERULUS* (At02270065_s1) and *ACT2* (At02329915_s1) or *ACT8* (At02270958) were used, or *ERU* and *TUB3* primers (for *arf7arf19*) were designed for SYBR green based qPCR (table S1). Three technical and three biological repeats were performed for each duplex PCR. Data was analysed using the ΔΔCt method.

Cloning of *ERULUS* and *Arabidopsis* transformation

Constructs were generated using gateway cloning. To construct the *ERUp::GFP* transgene, a 619bp sequence upstream of the translational start codon of ERULUS was amplified from col-0 genomic DNA using Platinum high fidelity DNA polymerase (Life Technologies). To create the *35S::ERU* overexpression construct and the *35S::ERU-GFP* overexpressed reporter construct, the entire *ERULUS* cds without stop codon was obtained by PCR. Primers: table S1. All DNA fragments were cloned to the pDONR207 entry vector, transformed in *E. coli* and the plasmids obtained from single colonies were verified by Sanger sequencing. Recombination was performed with isolated plasmid by LR reaction into the pGWB2 (35S promoter, no tag) or pGWB5 (35S promoter, C-terminal GFP) destination vectors. To obtain the translational protein-reporter transgene a genomic DNA segment containing the promoter and the coding region of ERULUS (3148 bp) was synthesized in the pENTR221 donor vector using The GeneArt® Gene Synthesis service (Life Technologies). This construct was recombined into the pGWB4 (no promoter, C-terminal GFP) binary vector. *Agrobacterium tumefaciens* C58 or LBA4404 strain transformed with the constructs was used to transform Col-0 and *eru Arabidopsis* plants using the floral dipping method [42]. *Agrobacterium* carrying the construct of interest was cultered in 5 mL liquid LB medium (10 g L^{-1} tryptone, 5 g L^{-1} NaCl, 5 g L^{-1} yeast extract) containing 50 µg l^{-1} kanamycin, 25 µg l^{-1} hygromycin, 25 µg l^{-1} rifampicin and 50 µg l^{-1} gentamycin for 48h at 28°C while shaking. Subsequently, using 1 mL of this pre-culture, a main culture was set up (24h, 28°C, shaking). This culture was centrifuged (8000g, 10min, 4°C) and the bacteria were resuspended in 500 mL transformation buffer (50 g L^{-1} sucrose, 0.74 g L^{-1} $MgCl_2$, 100 µL silwet-L77). The inflorescence of >50 *Arabidopsis* plants were dipped in this solution for 2.5min. Well-watered flower-dipped plants were covered with a plastic sheet for 24h to garuantee high humidity, after which they were left to fully mature and set seeds. Transformed seeds were selected by antibiotics resistance. Homozygous T_3 progeny was used for analysis.

ARF7/ARF19 ChIP-qPCR

Root cultures were pre-treated with 1 µM NAA to remove Aux/IAA proteins. DNA and protein complexes were cross-linked by submersing the tissue in 40 ml of Fixation Buffer (0,1 M sucrose, 50 mM NaCl, 10 mM KH_2PO_4, pH 7, 1 % formaldehyde, 10 µM MG132) and vacuum for 20 min. The reaction was stopped by adding cold glycine (0.125 M). Nuclei were isolated as described by Bowler *et al.* (2004) and re-suspended in 1 ml Sonication Buffer (10 mM potassium phosphate, pH 7, 0.1 M NaCl, 0.3% sarkosyl, 10 mM EDTA, 0.1 mM PMSF, 1X Sigma plant protease inhibitor cocktail)[43]. The chromatin was sonicated to yield fragments of 200-500 bp. 200 µl of sonicated chromatin was subsequently added to 1 ml Immuno-precipitation Buffer (50 mM Hepes, pH 7.5, 150 mM KCl, 5 mM

$MgCl_2$, 0.1% Triton X-100) and incubated with 3 µg of affinity purified anti-ARF19 or anti-ARF7 IgGs at 4°C on a slow-moving rotator for 4h. Anti-ARF7 antibody was produced in rabbits using an *E. coli*-expressed His-tagged antigenic region from aa 795-1039 [44]. The latter was used to affinity-purify the resulting antiserum. His-tagged ARF19 peptide (aa 541-720) was expressed in *E. coli* and used for antibody production in sheep [45]. The anti-ARF19 crude antisera were affinity-purified using Pierce Sulfo link resin as per their instructions.

Protein G Dynabeads® (Invitrogen) were added and incubated overnight. Elution and reverse cross-linking of the immunoprecipitated and non-immunoprecipitated chromatin samples were performed by heating to 95°C in 0.5 M NaCl solution for 20 min. Upon cooling, 4 µl of 20 mg ml^{-1} Proteinase K was added and the samples were incubated at 55 °C overnight, then at 65 °C for 6h. The magnetic beads were removed and DNA extracted from the remaining solution using phenol (buffered to pH 8):chloroform:isoamyl alcohol, 25:24:1. Precipitated DNA from the immunoprecipitated samples was re-suspended in 30 µl and the input DNA in 300 µl of water. Input and immunoprecipitated samples were diluted 10-fold and 5 µl thereof was used in a 12 µl volume reaction of SYBR green master mix and 1 µM each of forward and reverse oligonucleotides (SI table 1). The primers were designed based on the location of putative ARF binding sites. The putative 1500bp promoter region of ERULUS was examined for cis-elements using Place (http://www.dna.affrc.go.jp/PLACE/). All qPCR reactions were performed as triplicate technical replicates using a Roche LightCycler 480 qPCR machine. ChIP experiments are representative of three biological replicates.

Micro-Fourier transform IR spectroscopy (mFT-IR)

Six day old Col-0 and *eru* roots were dehydrated in ethanol and rehydrated overnight in distilled water. The dense RH collet at the hypocotyl-root junction was excised and dried at RT on a gold coated microscopy slide. FT-IR spectra were collected in an area of 30 x 30 µm where the stalks of multiple RHs overlapped using a Thermo Scientific Nicolet iN10 MX infrared imaging microscope equipped with a liquid nitrogen-cooled camera sensor coupled to the Thermo Scientific OMNIC Picta software. Spectra were collected in cooled reflection mode (dual transmission) ranging from 830 cm^{-1} to 1800 cm^{-1} with 3.857 cm^{-1} intervals. 64 spectra were co-added for each sample to increase the signal-to-noise ratio. The WT (n=72) and *eru* (n=46) spectra were baseline-corrected. Statistics were performed for each wavenumber using a student t-test (parametric) or kruskal wallis test (non-parametric) in R statistics or Multi-Experiment Viewer (MeV) respectively.

Immunolocalization and staining

Five day old Col-0 and *eru* seedlings grown on solid RH medium were covered with isotonic fixation buffer (50 mM PIPES, 5 mM $MgSO_4$, 5 mM EGTA, 4% paraformaldehyde, 0.1% glutaraldehyde, 1 % sucrose, pH 6.9) for 30 min, transferred to the same fixation buffer for 90 min and subsequently washed three times with 50 mM PIPES buffer (pH 6.9). Aspecific binding sites were blocked with PIPES buffer containing 3% BSA. After washing (PIPES 3x) seedlings were incubated overnight at 4°C with a 1:5 dilution of the Rat IgM primary antibody against methylesterified (LM20), de-esterified homogalacturonan (LM19) or xyloglucan (LM25)(Plant Probes, UK). After washing, the samples were incubated with 1:100 Alexa Fluor 488 Goat anti-Rat IgM secondary antibodies for 1 hour at RT. Washed samples were then mounted on a slide with PIPES buffer and visualized using a Nikon Eclipse E600 coupled to a D-Eclipse C1 confocal unit (Nikon, Brussels, Belgium), equipped with 488nm Argon laser and Plan Apo 60x (na 1.2) water immersion objective. The gain was adjusted so that no fluorescence signal was detectable for the negative control (no primary antibody), and subsequently images were collected for *eru* and WT roots using identical settings. For LM20 and LM19, fluorescence intensity plots were acquired from the RH stalk along 7 cross sectioning lines for each RH. Maximal intensity values were extracted from baselined (background subtracted) spectra.

Cellulose and pectin Ca^{2+} binding sites were stained using Direct Red 23 and propidium iodide

respectively. Five day old seedlings were fixed for 2h (see above), washed for 30 min, stained for 30 min using 0.01% w/v direct red 23 or 30 µM PI in PIPES, washed for 30 min and mounted in PIPES buffer for visualization using a D-Eclipse C1 confocal unit.
The thickness of the CW was measured on the obtained confocal images according to the following procedure. For each RH, intensity values along RH intersecting lines were obtained. The resulting plots show a background fluorescence level, and a subsequent peak in intensity corresponding to the signal coming from the CW. Each intensity plot was baselined (background subtracted) to make them comparable amongst the RH population, and a general intensity cutoff was set. The width of the intensity peak above the cutoff was calculated and considered to be an approximation for the cell wall width.

Pectin methylesterase activity assay

The PME activity was measured in accordance with [46], but with minor adjustments. Root tips were cut at the top of the differentiation zone and flash frozen. The soluble protein fraction was extracted from 10 mg of tissue by homogenization in 100 µL of 50 mM sodium phosphate buffer (containing 500 mM NaCl, protease inhibitor cocktail, pH 7.5) and subsequent centrifugation at 11,500 g (20 min, 4°C). PME activity was determined in triplicate immediately following extraction. The reaction was performed in an final volume of 110 µL, consisting of reaction mix (89,4 µL 50 mM phosphate buffer, 4 mM NAD^+, 0.35U formaldehyde dehydrogenase from *Pseudomonas* F1879 Sigma, 1U alcohol oxidase from *Pichia pastoris* A2404 Sigma, pH 7.5), 8 µL 0.5% pectin from citrus peel (P9135 Sigma) and 10 µL protein extract (samples), 4 µL recombinant pectinesterase from orange peel (positive control; P5400 Sigma), or 10 µL phosphate buffer (negative control). NADH absorbance was measured at 340 nm each 40 sec during 45 min (Biotek, Synergy MX), its concentration calculated using the extinction coefficient (6.220 M^{-1} cm^{-1}) and the result normalized to the total protein concentration [47]. PME assay results are representative of three biological replicates.

Microscopy

WT x ERU_{prom}::GFP plants were grown for 6 d on RH medium and placed on a slide with ddH_2O. Images were acquired using a Nikon Eclipse E600 coupled to a D-Eclipse C1 confocal unit (Nikon, Brussels, Belgium). Propidium iodide (0.1 mg ml^{-1}) was used as a counterstain. WT x *ERU*prom::GFP fluorescence profiles were extracted from images collected using a Nikon AZ100 multizoom macroscope coupled to 488nm fluorescence unit.
ERU-GFP subcellular localization was visualized using the above mentioned confocal microscope and a 60x water immersion objective (for overview images), and a Zeiss Axiovert 200 (Carl Zeiss, Jena, Germany) equipped with a microlens-enhanced dual spinning disk confocal system, a three-line argon-krypton laser and a 63x oil immersion lens for higher resolution images (Ultraview ERS; PerkinElmer, Seer Green, UK). For the latter, 4-6 d old seedlings were mounted in liquid RH growth medium and Z-stacks were collected from actively growing RHs using a step size of 0.4-1 µm. FIJI was used to generate 3D renderings and maximal projections of the acquired Z-stacks (Volume viewer and 3D project plugins). For timelapse acquisition, 5-d old seedlings were grown on slides overlayed with a thin layer of solid RH growth medium. The roots were overlaid with a coverslip and left to recover for 1h prior imaging at 4 sec intervals.
Pectin Ca^{2+} binding site oscillations were visualized using propidium iodide staining, as described by Rounds et al. (2011), with small adjustments [9]. WT and *eru* (-/-) seedlings were grown in square petri dishes for 4-5 days on standard RH growth medium overlaying microscopy slides. The slides were excised from the medium, the seedlings were covered with a 10 µM PI solution in liquid RH growth medium, overlayed with a large coverslip, and left to recover for 30 min in a climate controlled environment (22°C). A fully automated Nikon Ti wide-field microscope (Nikon Instruments, Paris, France), with a 60x (na 1.2) oil immersion objective was used to collect PI fluorescence and transmitted

light images every 3 seconds for 10-20 min at a resolution of 0.12 µm pixel^{-1}. Samples were illuminated with a Lumencor Spectra-X solid state light source (550/15nm; laser power 5%) and detected through a multiple dichroic and 620/40 bandpass filter on a CS-Ri2 scientific CMOS camera. Image acquisition was performed using Nikon NIS Elements with exposure times set to 100 ms (transmission) and 500 ms (fluorescence), closing the shutters in between consecutive acquisitions. RHs showing normal cytoplasmic streaming and the presence of a dynamic clear zone at the tip were selected for imaging. The acquired PI fluorescence time series for individual RHs were imported in FIJI as a stack and all frames were aligned with the stackreg plugin using Rigid registration. As such, a time series was acquired in which the tip was stationary from frame to frame, allowing the use of a single region of interest (ROI) for data extraction. For each frame, the average fluorescence intensity of the background and a 1.4 µm² ROI at the RH tip were measured. For each timepoint, the background signal intensity was subtracted from the apical PI fluorescence intensity. To correct for bleaching, the obtained PI fluorescence time series were de-trended in Autosignal v1.7 (Systat Software, Inc.). A Fast Fourier Transform Radix 2 algorithm was employed in Autosignal v1.7 to perform frequency analysis of the acquired oscillograms. Hence, the PI fluorescence time series for individual RHs were transformed in order to show the PI oscillatory behaviour as a spectrum of frequencies and their corresponding amplitude. For each oscillogram, the well-defined highest amplitude frequencies were isolated to describe the main PI oscillatory behaviour. Kymographs were constructed using the multi kymograph plugin in FIJI.

Phosphoproteome analysis

Briefly, 100 mg of finely ground plant material was suspended in homogenization buffer containing 50 mM Tris-HCl buffer (pH 8), 30% sucrose, 5 mM EDTA, and 1 mM DTT in Milli-Q water and appropriate amounts of the cOmplete^{TM} protease inhibitor mixture (Roche) and the PhosSTOP^{TM} phosphatase inhibitor mixture (Roche). After sonication and removal of cell debris by centrifugation, a methanol/chloroform precipitation was carried out with the supernatant as described previously [48]. Pellets were washed with 80% acetone and re-suspended in 8 M urea. Alkylation of cysteines was carried out in the presence of 15 mM tris(carboxyethyl)phosphine (TCEP, Pierce) and 30 mM iodoacetamide (Sigma-Aldrich). Three mg of protein material was digested with 10 µg of MS grade endoproteinase-Lys-C (Wako Chemicals GmbH), followed by an overnight digestion with 30 µg of trypsin (Promega) at 37°C. The digest was acidified to pH ≤ 3 with trifluoroacetic acid (TFA) and desalted using SampliQ C18 SPE cartridges (Agilent) according to the manufacturer's guidelines. The desalted peptides were fully dried in a vacuum centrifuge and then re-suspended in 500 µl of loading solvent [80% (v/v) acetonitrile, 6% (v/v) TFA], from which 100 µl were kept for proteome analysis while 400 µl were proceeded further with phospho-enrichment using MagReSyn® Ti-IMAC (ReSyn Biosciences) as described previously [48]. Samples were vacuum dried and dissolve in 30 µl 2% (v/v) acetonitrile and 0.1% (v/v) TFA prior to LC-MS/MS analysis.

Each sample was analyzed via LC-MS/MS on an Ultimate 3000 RSLC nano LC (Thermo Fisher Scientific, Bremen, Germany) in-line connected to a Q Exactive mass spectrometer (Thermo Fisher Scientific). The peptides were first loaded on a trapping column (made in-house, 100 µm internal diameter (I.D.) × 20 mm, 5 µm beads C18 Reprosil-HD, Dr. Maisch, Ammerbuch-Entringen, Germany). After flushing the trapping column, peptides were loaded in solvent A (0.1% formic acid in water) on a reverse-phase column (made in-house, 75 µm I.D. x 250 mm, 1.9 µm Reprosil-Pur-basic-C18-HD beads, Dr. Maisch, packed in the needle) and eluted by an increase in solvent B (0.1% formic acid in acetonitrile) in a linear gradient from 2% solvent B to 55% solvent B in 120 minutes, followed by a 5-min washing step with 99% solvent B, all at a constant flow rate of 300 nL min^{-1}. The mass spectrometer was operated in data-dependent, positive ionization mode, automatically switching between MS and MS/MS acquisition for the 5 most abundant peaks in a given MS spectrum. The source voltage was set at 4.1 kV and the

capillary temperature at 275°C. One MS1 scan (m/z 400−2,000, AGC target 3 × 106 ions, maximum ion injection time 80 ms), acquired at a resolution of 70,000 (at 200 m/z), was followed by up to 5 tandem MS scans (resolution 17,500 at 200 m/z) of the most intense ions fulfilling predefined selection criteria (AGC target 5 × 104 ions, maximum ion injection time 80 ms, isolation window 2 Da, fixed first mass 140 m/z, spectrum data type: centroid, under-fill ratio 2%, intensity threshold 1.3xE4, exclusion of unassigned, 1, 5-8, >8 positively charged precursors, peptide match preferred, exclude isotopes on, dynamic exclusion time 12 s). The HCD collision energy was set to 25% Normalized Collision Energy and the polydimethylcyclosiloxane background ion at 445.120025 Da was used for internal calibration (lock mass).

Database search and data analysis was performed using MaxQuant v.1.5.4.1 and Perseus 1.5.5.3, respectively as described previously [48]. For phosphoproteome data (*eru* data set), only phosphosites with localization probabilities larger than 0.75 were retained for analysis. Two-sample T-tests were performed with a cut-off p-value of 0.05. For NAA phosphoproteomics, a two-sample t-test was carried out with permutation-based false discovery rate (FDR) < 0.05 and 250 randomizations to correct for multiple-hypothesis testing.

Bioinformatic analysis

A search for non-redundant *A. thaliana* proteins with sequence homology to the 27 AA signal peptide sequence was performed using the pBLAST algorithm for short input sequences. The corresponding FASTA sequences were retrieved for all 100 peptide hits using the NCBI batch entrez tool and blasted against the annotated *A. thaliana* protein library using the Tair WU-BLAST2 tool (www.arabidopsis.org/wublast/index2.jsp) to identify the unique proteins corresponding to the aligned peptides. The AGI codes of the 51 unique proteins originating from the top 100 BLAST hits were subsequently used for Gene Ontology enrichment analysis (cellular component annotation database; Bonferroni correction). The whole protein FASTA sequences corresponding to the 51 identified proteins were retrieved using the Tair bulk data retrieval tool, and subsequently used for motif analysis. MEME version 4.11.2 was used for motif discovery, and set to compute the 3 most prominent motifs with a width of 6-20 AA. Data on root cell specific transcription of *ARF7* and *ARF19* was collected from the eFP browser [49].

QUANTIFICATION AND STATISTICAL ANALYSIS

Image analysis was performed in Fiji. Detailed procedures for image processing are described in the method details. Statistics were performed in Perseus version 1.5.5.3 (phosphoproteomics) or R [50]. All data er represented as mean ± SEM, and n indicates the sample size as the number of independent samples. The sample size for individual experiments is stated in the figure captions and method details. Significance ($\alpha = 0.05$) was assessed by two-way analysis of variance (ANOVA; parametric) using linear mixed-effects models followed by a TukeyHSD (for pairwise statistical analysis), or Kruskal-Wallis tests (non-parametric). MicroFT-IR data were analyzed in MultiExperiment Viewer (www.tm4.org/mev, version 4.8.1) using Kruskal-Wallis (for non-parametric distributed wavenumbers) or student t-tests (for normally distributed wavenumbers). Normality was assessed by Shapiro Wilkinson tests (non-normal distribution < W=0.95 < normal distribution). Correlation analysis was performed using the non-parametric Spearman's rank correlation test.

Supplemental movie legends

movie S1. Representative 3D rendering of ERU-GFP subcellular protein localization in growing *Arabidopsis* RH bulge, Related to Figure 2. Native and false color representations rotating around X and Y axis.

movie S2. Representative 3D rendering of ERU-GFP subcellular protein localization in a tip growing *Arabidopsis* RH, Related to Figure 2. Native and false color representations rotating around X and Y axis.

movie S3. Representative spinning disk timelapse showing the evolution of ERU-GFP abundance at the growing RH tip, Related to Figure 2.

movie S4. Representative 9 min time-lapse movie of pectin Ca^{2+} egg box oscillations in WT and *eru* tip growing *Arabidopsis* RHs, visualized by *in vivo* propidium iodide staining, Related to Figure 5.

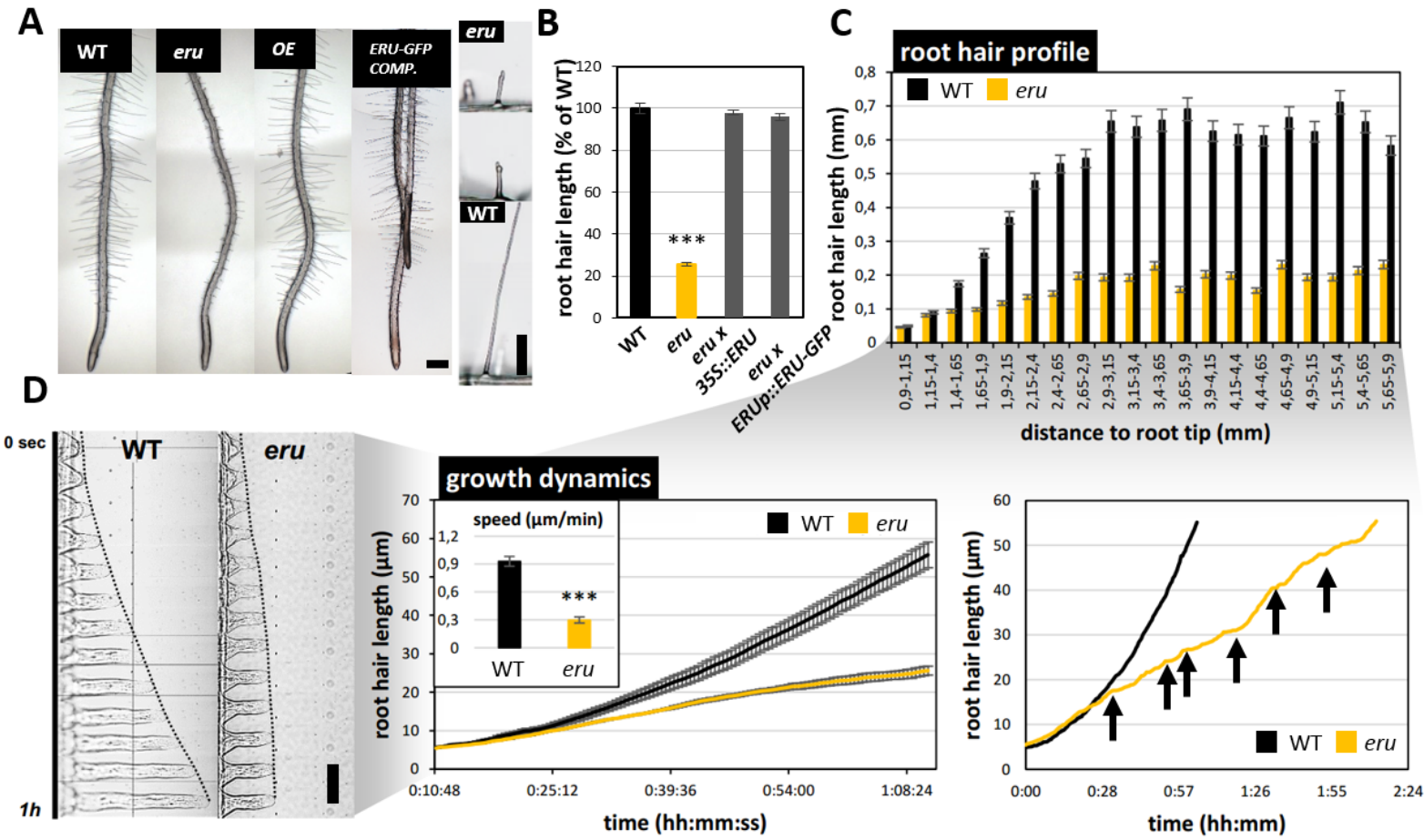
A
WT
eru
OE
ERU-GFP COMP.
eru
WT
B
root hair length (% of WT)
120
100
80
60
40
20
0
***
WT
eru
eru x 35S::ERU
eru x ERUp::ERU-GFP
C
root hair profile
WT
eru
root hair length (mm)
0,8
0,7
0,6
0,5
0,4
0,3
0,2
0,1
0
0,9-1,15
1,15-1,4
1,4-1,65
1,65-1,9
1,9-2,15
2,15-2,4
2,4-2,65
2,65-2,9
2,9-3,15
3,15-3,4
3,4-3,65
3,65-3,9
3,9-4,15
4,15-4,4
4,4-4,65
4,65-4,9
4,9-5,15
5,15-5,4
5,4-5,65
5,65-5,9
distance to root tip (mm)
D
0 sec
WT
eru
1h
growth dynamics
root hair length (µm)
70
60
50
40
30
20
10
0
speed (µm/min)
1,2
0,9
0,6
0,3
0
***
WT
eru
WT
eru
0:10:48
0:25:12
0:39:36
0:54:00
1:08:24
time (hh:mm:ss)
root hair length (µm)
60
50
40
30
20
10
0
WT
eru
0:00
0:28
0:57
1:26
1:55
2:24
time (hh:mm)

Figure 1

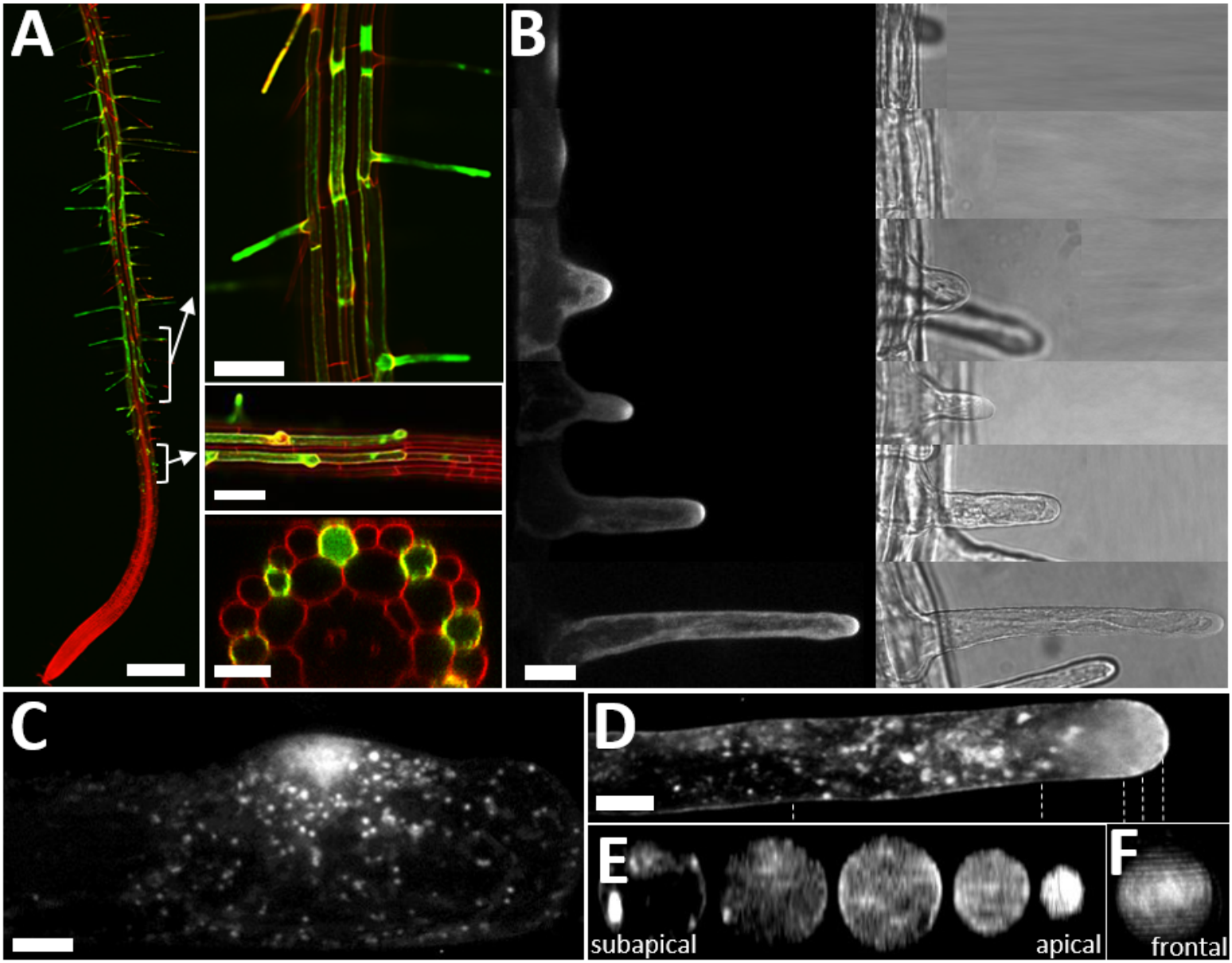

Figure 2

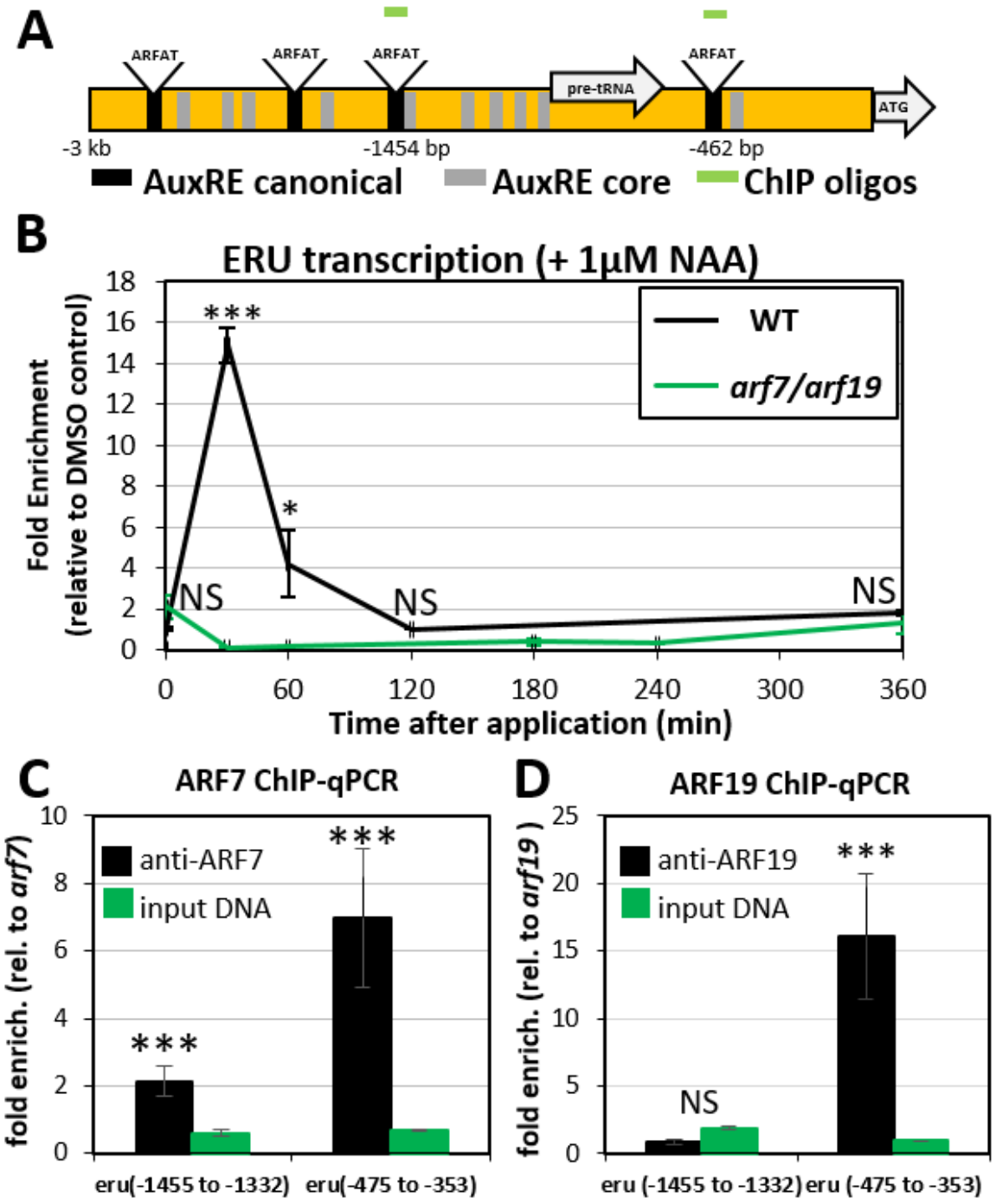
A
ARFAT
ARFAT
ARFAT
pre-tRNA
ARFAT
ATG
-3 kb
-1454 bp
-462 bp
AuxRE canonical
AuxRE core
ChIP oligos
B
ERU transcription (+ 1µM NAA)
Fold Enrichment (relative to DMSO control)
WT
arf7/arf19
***
*
NS
NS
NS
Time after application (min)
C
ARF7 ChIP-qPCR
fold enrich. (rel. to arf7)
anti-ARF7
input DNA
***
***
eru(-1455 to -1332)
eru(-475 to -353)
D
ARF19 ChIP-qPCR
fold enrich. (rel. to arf19)
anti-ARF19
input DNA
***
NS
eru (-1455 to -1332)
eru (-475 to -353)

Figure 3

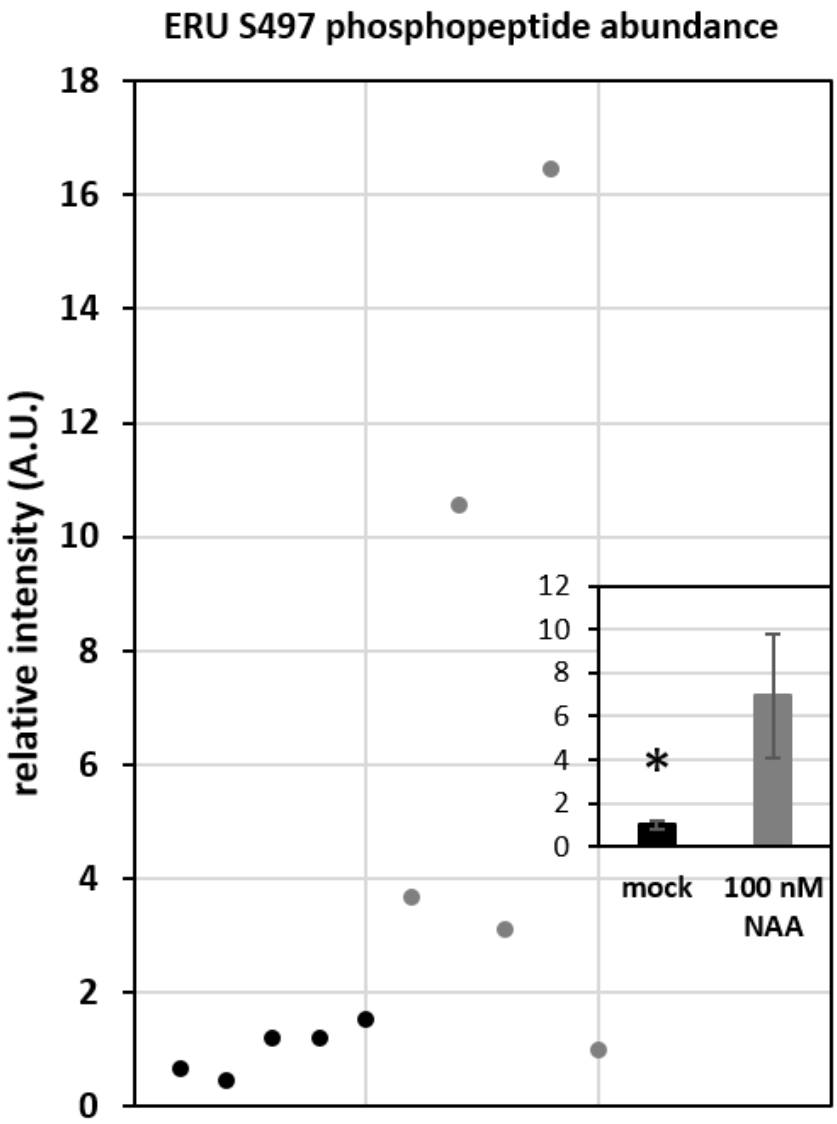
ERU S497 phosphopeptide abundance
relative intensity (A.U.)
18
16
14
12
10
8
6
4
2
0
12
10
8
6
4
2
0
*
mock
100 nM NAA

Figure 4

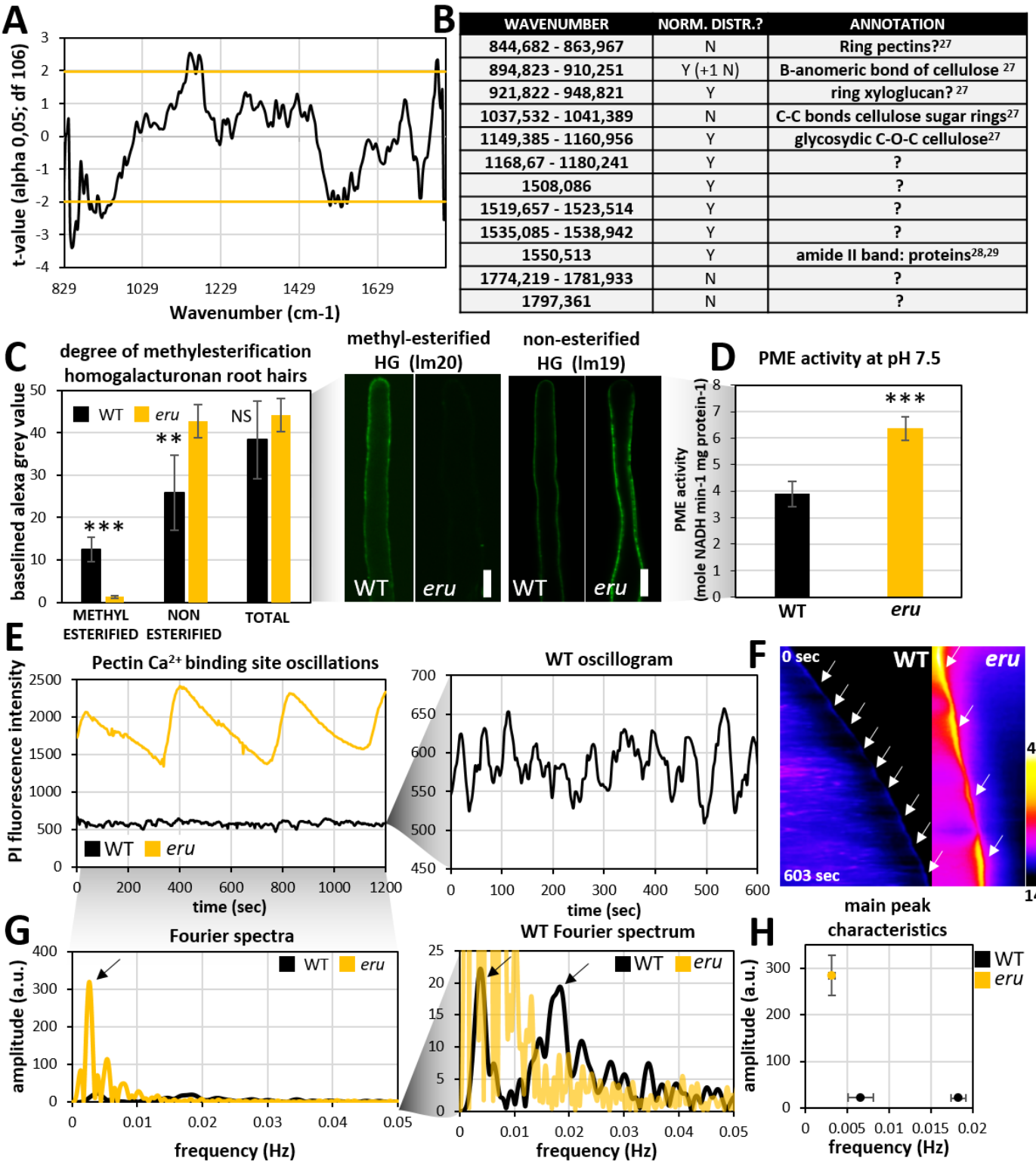

WAVENUMBER	NORM. DISTR.?	ANNOTATION
844,682 - 863,967	N	Ring pectins?[27]
894,823 - 910,251	Y (+1 N)	B-anomeric bond of cellulose [27]
921,822 - 948,821	Y	ring xyloglucan? [27]
1037,532 - 1041,389	N	C-C bonds cellulose sugar rings[27]
1149,385 - 1160,956	Y	glycosydic C-O-C cellulose[27]
1168,67 - 1180,241	Y	?
1508,086	Y	?
1519,657 - 1523,514	Y	?
1535,085 - 1538,942	Y	?
1550,513	Y	amide II band: proteins[28,29]
1774,219 - 1781,933	N	?
1797,361	N	?

Figure5

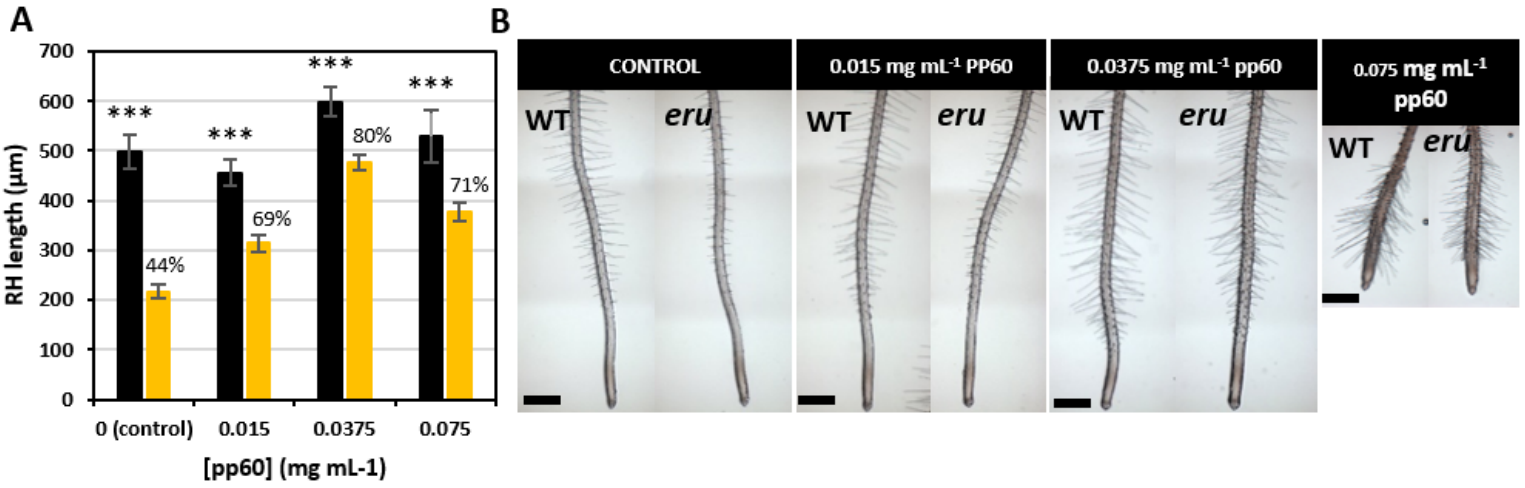
A
B
RH length (µm)
700
600
500
400
300
200
100
0
***
***
***
***
44%
69%
80%
71%
0 (control)
0.015
0.0375
0.075
[pp60] (mg mL-1)
CONTROL
0.015 mg mL-1 PP60
0.0375 mg mL-1 pp60
0.075 mg mL-1 pp60
WT
eru

Figure 6

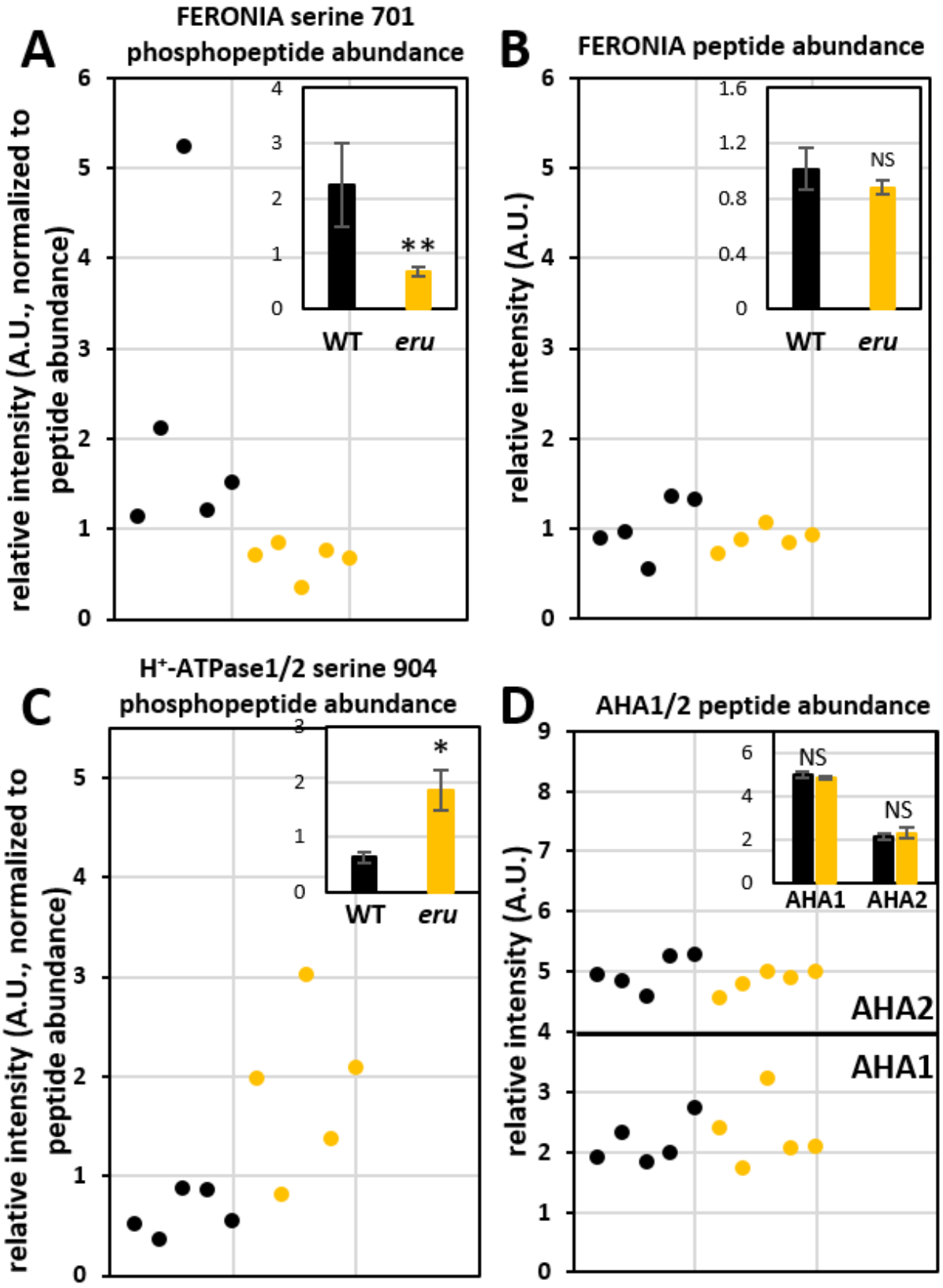
A
FERONIA serine 701 phosphopeptide abundance
relative intensity (A.U., normalized to peptide abundance)
**
WT
eru
B
FERONIA peptide abundance
relative intensity (A.U.)
NS
WT
eru
C
H+-ATPase1/2 serine 904 phosphopeptide abundance
relative intensity (A.U., normalized to peptide abundance)
*
WT
eru
D
AHA1/2 peptide abundance
relative intensity (A.U.)
NS
NS
AHA1
AHA2
AHA2
AHA1

Figure 7

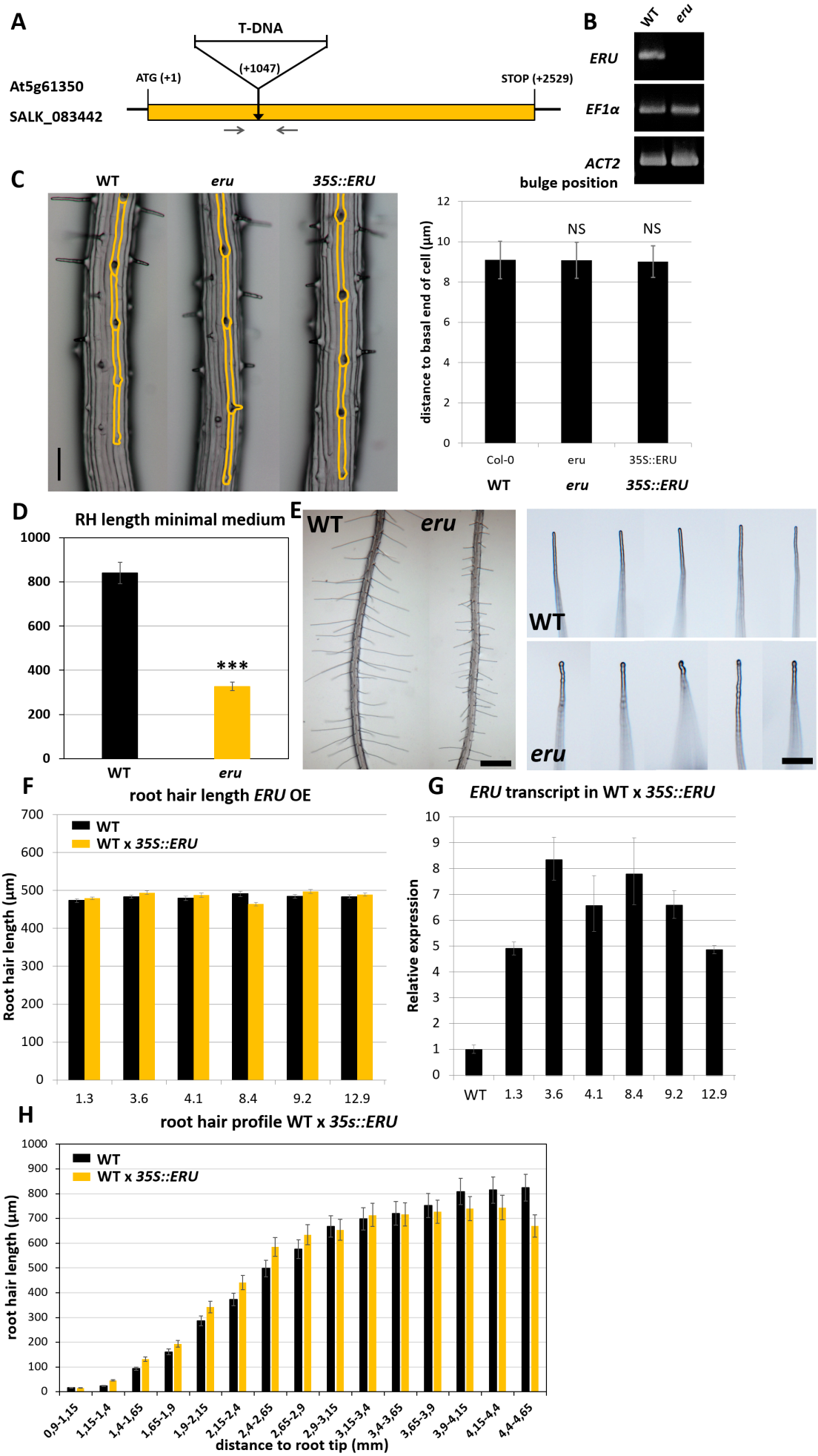
A
T-DNA
(+1047)
ATG (+1)
STOP (+2529)
At5g61350
SALK_083442
B
WT
eru
ERU
EF1α
ACT2
C
WT
eru
35S::ERU
bulge position
distance to basal end of cell (µm)
NS
NS
Col-0
eru
35S::ERU
WT
eru
35S::ERU
D
RH length minimal medium
***
WT
eru
E
WT
eru
WT
eru
F
root hair length ERU OE
WT
WT x 35S::ERU
Root hair length (µm)
1.3
3.6
4.1
8.4
9.2
12.9
G
ERU transcript in WT x 35S::ERU
Relative expression
WT
1.3
3.6
4.1
8.4
9.2
12.9
H
root hair profile WT x 35s::ERU
WT
WT x 35S::ERU
root hair length (µm)
0,9-1,15
1,15-1,4
1,4-1,65
1,65-1,9
1,9-2,15
2,15-2,4
2,4-2,65
2,65-2,9
2,9-3,15
3,15-3,4
3,4-3,65
3,65-3,9
3,9-4,15
4,15-4,4
4,4-4,65
distance to root tip (mm)

Figure S1. Geno- and phenotyping of the *eru* (-/-) mutant and *ERU* overexpression line, Related to Figure 1.

(A) graphical representation of the T-DNA insertion site in SALK_083442 (*erulus*; Nottingham Arabidopsis Stock Centre) and the position of the primers used for RT-PCR. (B) semi-quantitative RT-PCR of *ERU* transcription in WT and *eru* (-/-) 6d old roots. (C) *Eru* (-/-) does not affect bulge positioning. Representative DIC images of WT, *eru* and WT x *35S::ERU* roots in the region of bulge formation. Orange outlines depict individual root epidermal cells. Scale bar, 100 µm. Bar plot showing distance of the bulge to the basal end of the epidermal cell. Bars represent the average of at least 4 measured cells per 5 roots for each line. Error bars represent SE (n=5). (D) WT and *eru* RH length when grown on minimal medium. Bars represent the average of the 5 longest RHs of >15 roots per line (n=3). (E) representative close-up of minimal medium grown WT and *eru* RH tips showing normal WT RH morphology but bulged/swollen *eru* RHs. (F-H) Characterization of *ERU* overexpression lines. (F) Final RH length in WT (Col-0) and WT x *35S::ERU* roots of 6 independent lines. Bar graphs represent means with SE, n=3. (G) Relative ERU transcript abundance in roots of 6 independent WT x *35S::ERU* lines. Bar graphs represent means with SE, n=9. (H) Root hair profile of WT and WT x *35S::ERU* overexpression lines (n≥3). Error bars represent SE. Significance codes p-value: 0.05 '*' 0.01 '**' <0.001 '***'.

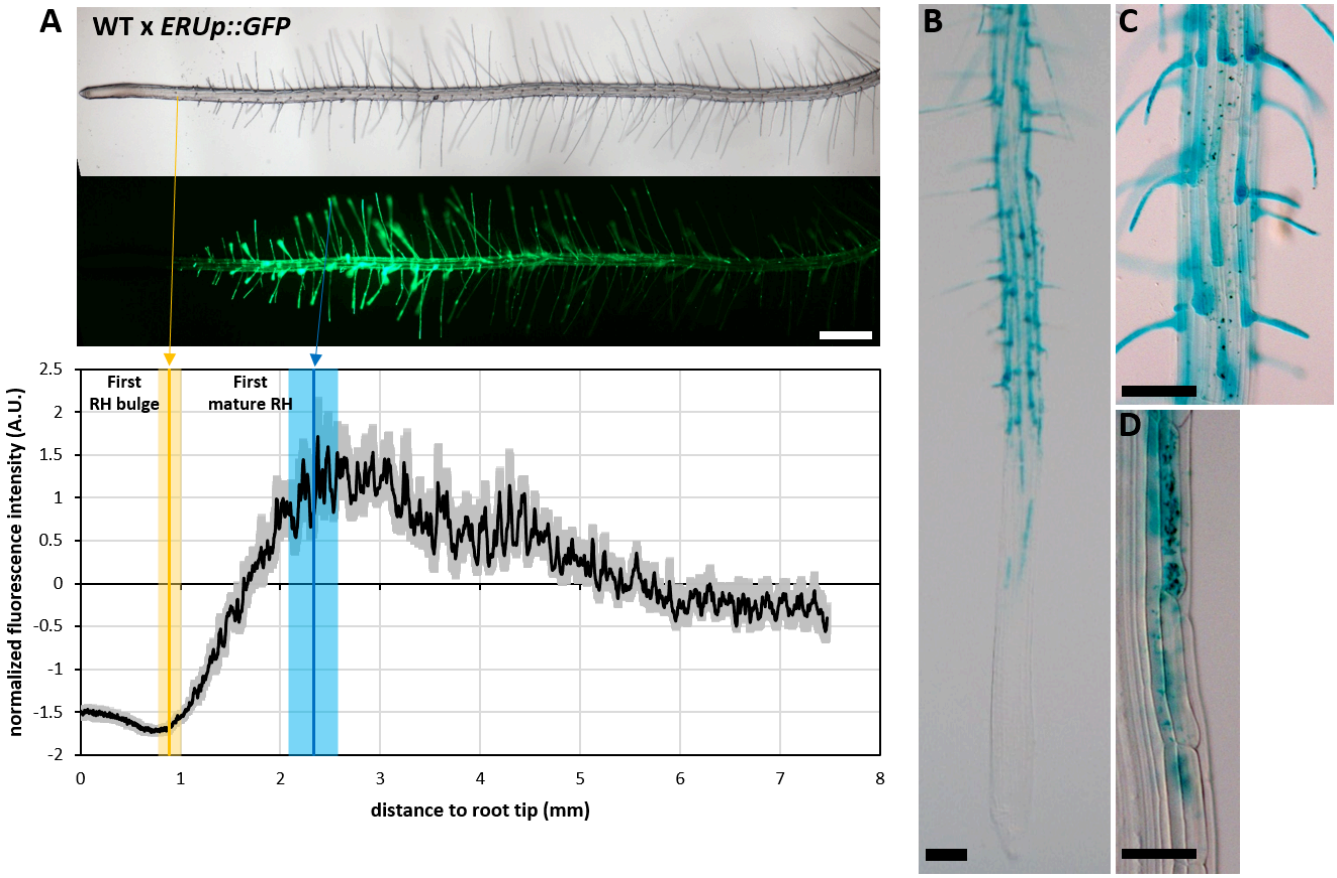

Figure S2. *ERU* is expressed in trichoblast cell files specifically during RH tip growth, Related to Figure 2.

(A) Representative brightfield and fluorescence images of a 7d old WT x *ERUp::GFP* root and graph representing GFP fluorescence level along the roots axis (scale bar, 500 µm). The average position of the first RH bulge (orange) and the first mature RH (blue) are depicted. Error bars represent SE (n=9). (B-D) Representative DIC images of GUS stained plants expressing *ERUp::GUS*. (B) overview of a 7d old root (scale bar, 100 µm). (C) close-up of GUS stained trichoblasts in the differentiation zone (scale bar, 100 µm). (D) close-up of a GUS stained epidermal cell file in early RH development (scale bar, 50 µm). GUS staining is visible before bulge formation.

A

Bonferroni corrected GO enrichment analysis

	Arabidopsis thaliana (REF)	upload_1 (▿ Hierarchy NEW!)				
GO cellular component complete	#	#	expected	Fold Enrichment	+/-	P value
extracellular region	2558	17	4.68	3.64	+	7.51E-04
Unclassified	5344	5	9.77	.51	-	0.00E00

B

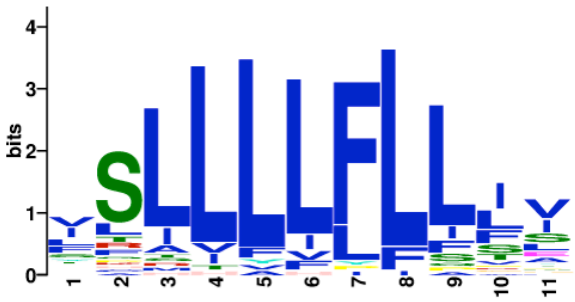

C

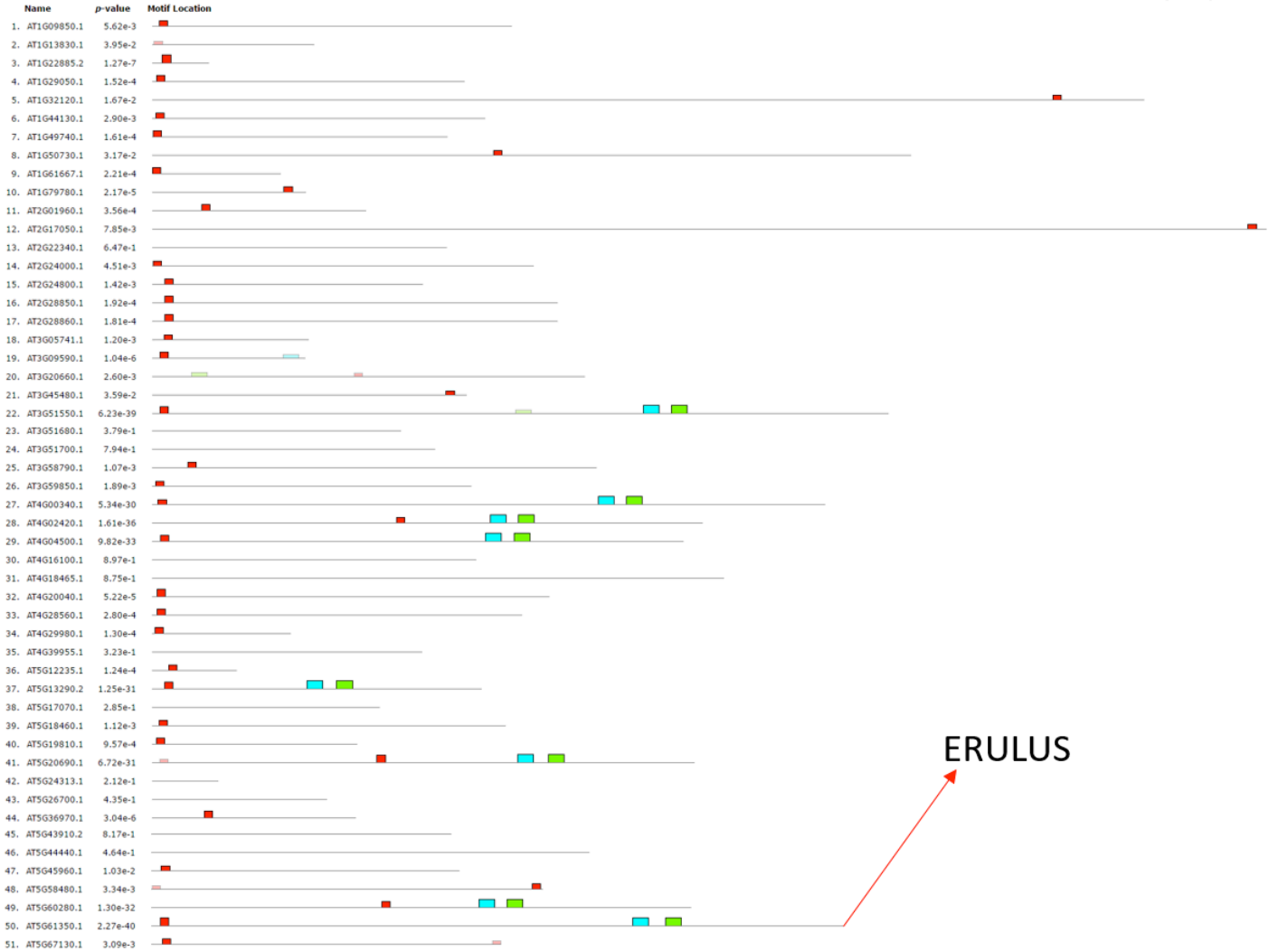

Figure S3. A motif identified in the ERU signal peptide is conserved amongst proteins which are potentially targeted to the extracellular region, Related to Figure 2.

(A) GO enrichment analysis of the 51 unique proteins identified from a BLAST search for non-redundant protein sequences similar to the ERU signal peptide. (B) highly conserved motif identified in the protein sequences corresponding to the 51 unique proteins identified from a BLAST search for non-redundant protein sequences similar to the ERU signal peptide. (C) Location of the motif in the whole protein sequence of the 51 proteins that were analysed. the ERU sequence is marked (red arrow).

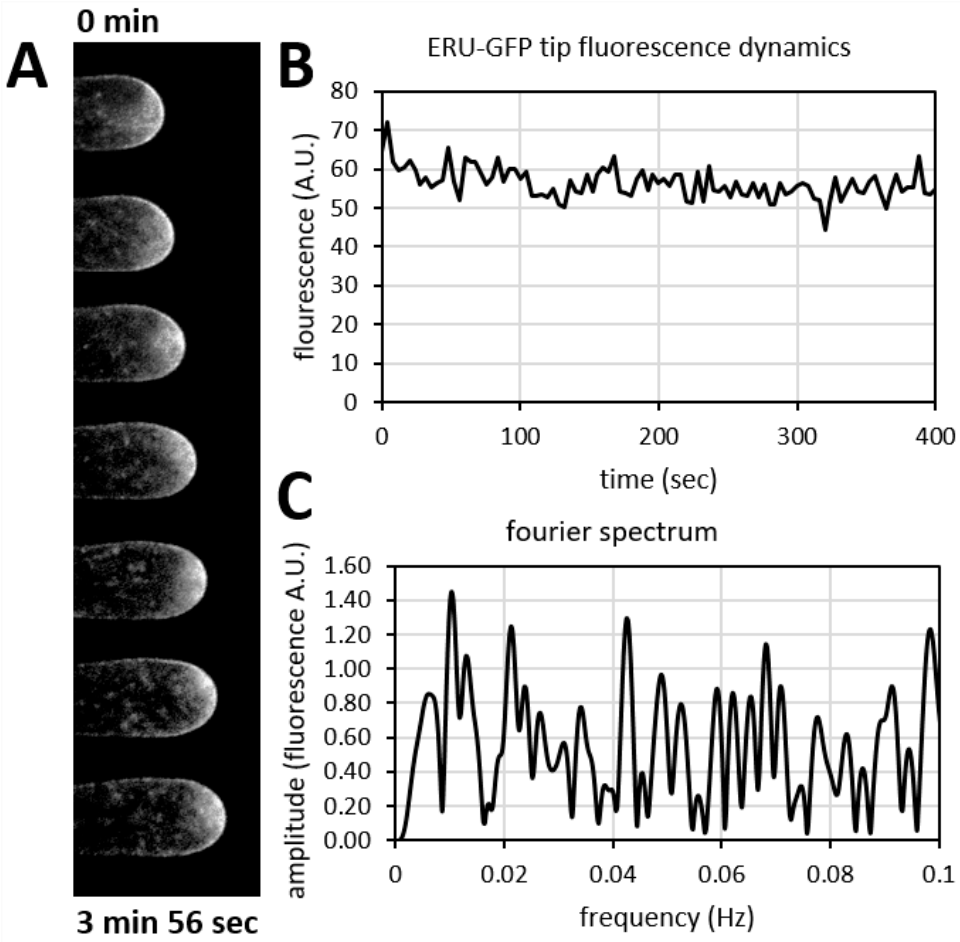

Figure S4. ERU plasma membrane protein abundance displays no oscillatory behaviour, Related to Figure 2.

(A) representative growing RH tip showing ERU-GFP localization to the apical PM. (B) Representative graph showing the evolution of ERU-GFP fluorescence intensity during a 400s acquisition. (C) Fourier spectrum of apical ERU-GFP abundance time plot showing no distinct oscillatory frequency.

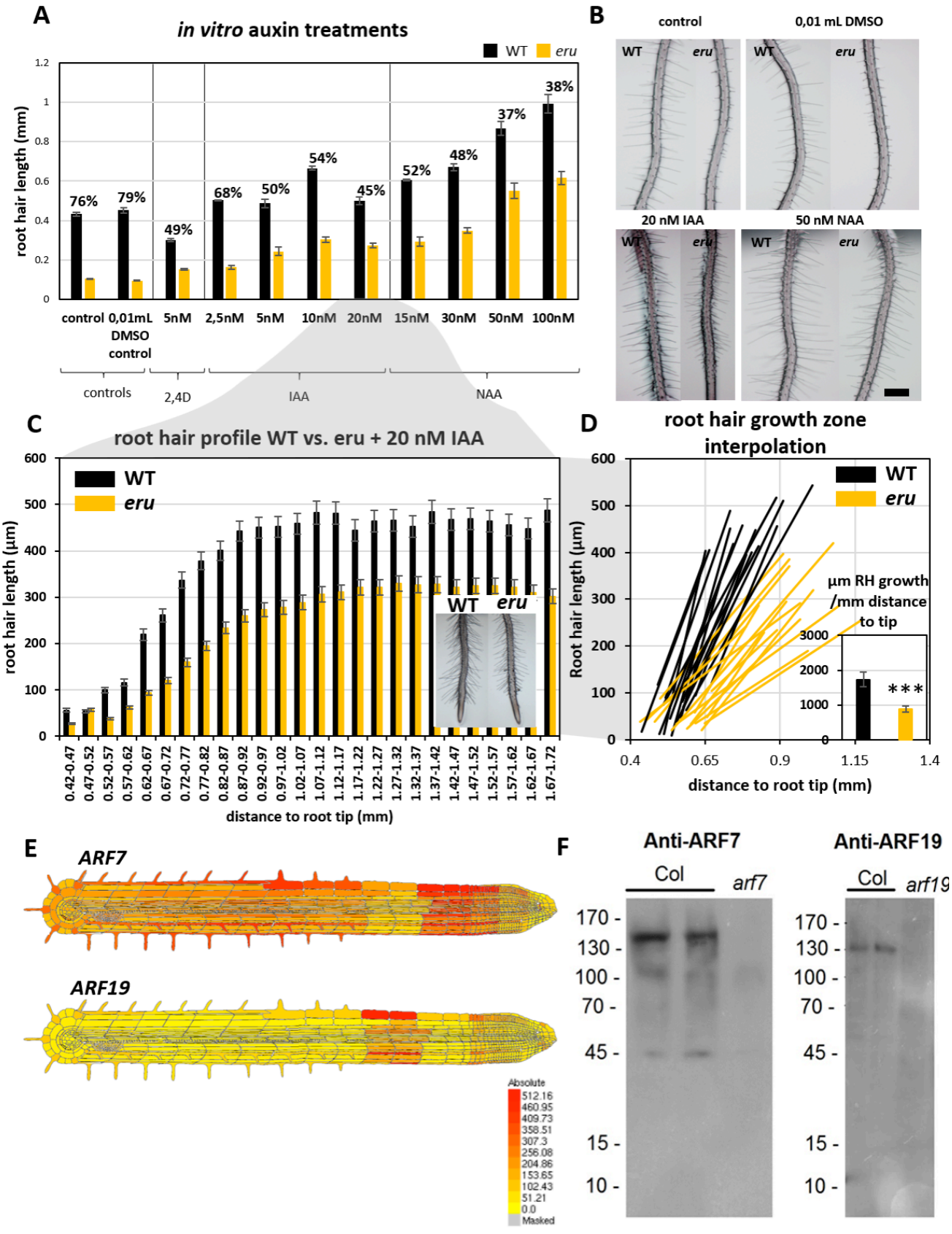
A
in vitro auxin treatments
WT
eru
root hair length (mm)
76%
79%
49%
68%
50%
54%
45%
52%
48%
37%
38%
control
0,01mL DMSO control
5nM
2,5nM
5nM
10nM
20nM
15nM
30nM
50nM
100nM
controls
2,4D
IAA
NAA
B
control
0,01 mL DMSO
20 nM IAA
50 nM NAA
C
root hair profile WT vs. eru + 20 nM IAA
root hair length (µm)
distance to root tip (mm)
D
root hair growth zone interpolation
Root hair length (µm)
µm RH growth /mm distance to tip
***
distance to root tip (mm)
E
ARF7
ARF19
Absolute
512.16
460.95
409.73
358.51
307.3
256.08
204.86
153.65
102.43
51.21
0.0
Masked
F
Anti-ARF7
Anti-ARF19
Col
arf7
arf19
170 -
130 -
100 -
70 -
45 -
15 -
10 -

Figure S5. Effect of auxin on the *eru* phenotype, ARF7/19 root transcription, anti-ARF7/19 western blots, Related to Figure 3.

(A-D) Supplementation with auxin cannot rescue the *eru* phenotype. WT and *eru* seedlings were transferred to plates containing different concentrations of IAA, NAA and 2,4D. (A) Bar plots showing the effect of auxin addition on the average length of newly emerged RHs. At least 10 RHs were measured for 30 roots per treatment and line. (B) representative images of auxin treated WT and *eru* roots. Scale bar, 0.5 mm. (C) *eru* and WT RH profiles after 20 nM IAA supplementation (n=24). (D) Linear interpolation of the RH growth zone. Each line represents the region of linear RH elongation for a single root (n=24). Average RH growth velocity, derived from the slope of individual root RH growth zone interpolations (n=24). Error bars represent SE. (E) *ARF7* and *ARF19* are transcribed in trichoblasts. Root cell-specific transcription of *ARF7* (right) and *ARF19* (left) as extracted from public transcriptomics data [S1]. Yellow and red represents low and high transcription respectively. (F) Anti-ARF7 and anti-ARF19 antibodies are antigen-specific. Western blots using polyclonal anti-ARF7 (rabbit) and anti-ARF19 (sheep) with root culture nuclei preparations of WT and *arf7* or *arf19 Arabidopsis* plants. In Col-0 samples, specific staining is observed at expected molecular weights (~130 kDa). ARF7 and ARF19 staining is absent in *arf7* and *arf19* knock-out mutants respectively.

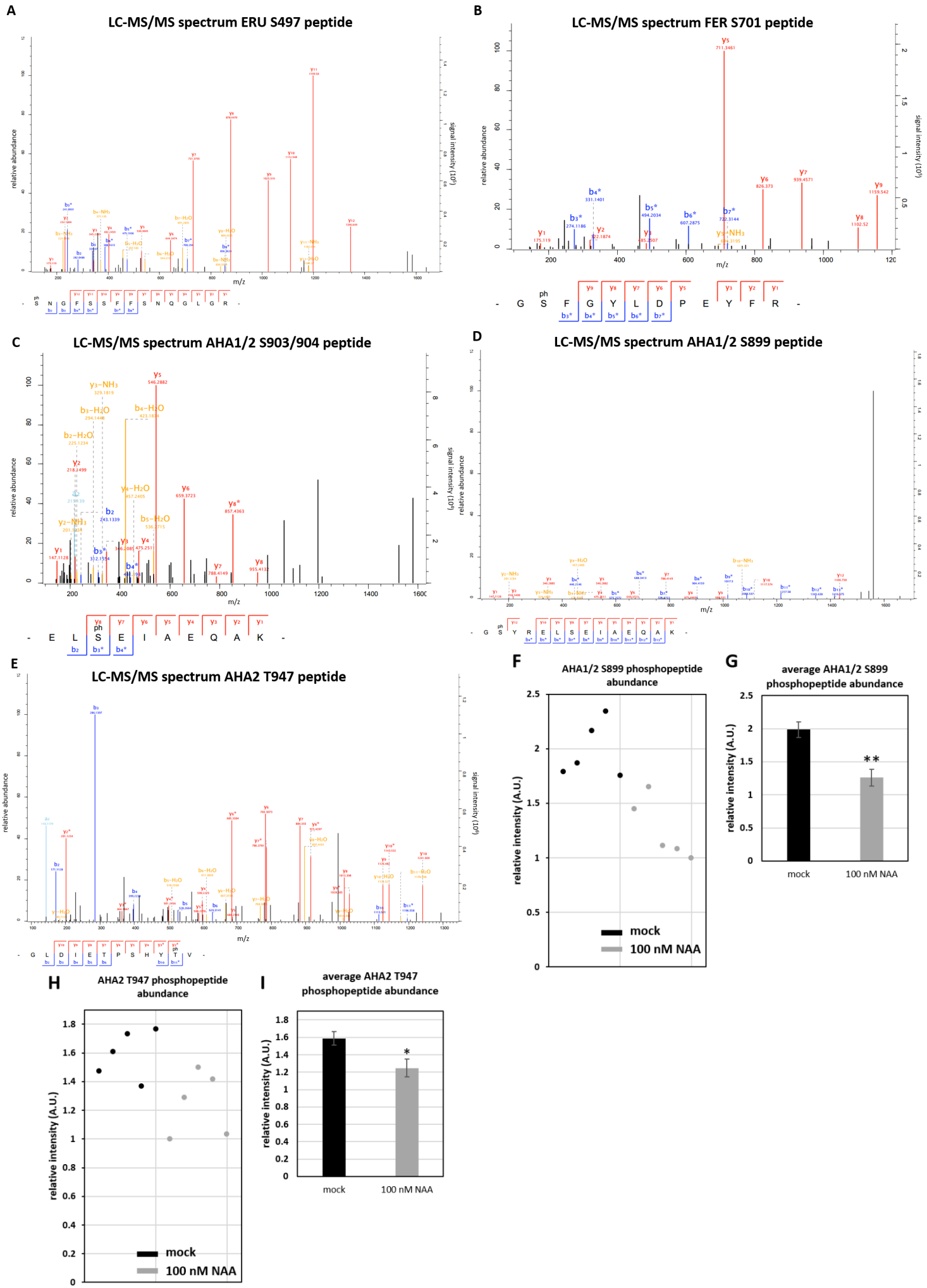
A
LC-MS/MS spectrum ERU S497 peptide
relative abundance
signal intensity (10⁵)
m/z
- S N G F S S F F S N Q G L G R -
B
LC-MS/MS spectrum FER S701 peptide
relative abundance
signal intensity (10⁵)
m/z
- G S F G Y L D P E Y F R -
C
LC-MS/MS spectrum AHA1/2 S903/904 peptide
relative abundance
signal intensity (10⁵)
m/z
- E L S E I A E Q A K -
D
LC-MS/MS spectrum AHA1/2 S899 peptide
relative abundance
m/z
- G S Y R E L S E I A E Q A K -
E
LC-MS/MS spectrum AHA2 T947 peptide
relative abundance
signal intensity (10⁵)
m/z
- G L D I E T P S H Y T V -
F
AHA1/2 S899 phosphopeptide abundance
relative intensity (A.U.)
mock
100 nM NAA
G
average AHA1/2 S899 phosphopeptide abundance
relative intensity (A.U.)
**
mock
100 nM NAA
H
AHA2 T947 phosphopeptide abundance
relative intensity (A.U.)
mock
100 nM NAA
I
average AHA2 T947 phosphopeptide abundance
relative intensity (A.U.)
*
mock
100 nM NAA

Figure S6. Annotated LC-MS/MS spectra for the identified phosphopeptides and AHA1/2 phosphorylation is response to auxin, Related to Figure 4.

LC-MS/MS spectra for the (A) ERU S497, (B) FER S701, (C) AHA2 S904, (D) AHA2 S899 and (E) AHA2 T947 peptide. AHA1/2 and AHA2 are dephosphorylated at serine 899 and threonine 947 respectively in response to auxin. (F) abundance of the AHA1/2 S899 associated phosphopeptide in individual replicates of mock treated (black dots) and auxin treated (grey dots) root samples. (G) average S899 phosphopeptide abundance (n=5). (H) abundance of the AHA2 T947 associated phosphopeptide in individual replicates of mock treated (black dots) and auxin treated (grey dots) root samples. (I) average T947 phosphopeptide abundance (n=5). Graph and statistics based on centered log2 transformed values for the complete data set (unpublished results). Error bars represent SE. Significance codes p-value: 0.05 '*' 0.01 '**' <0.001 '***'.

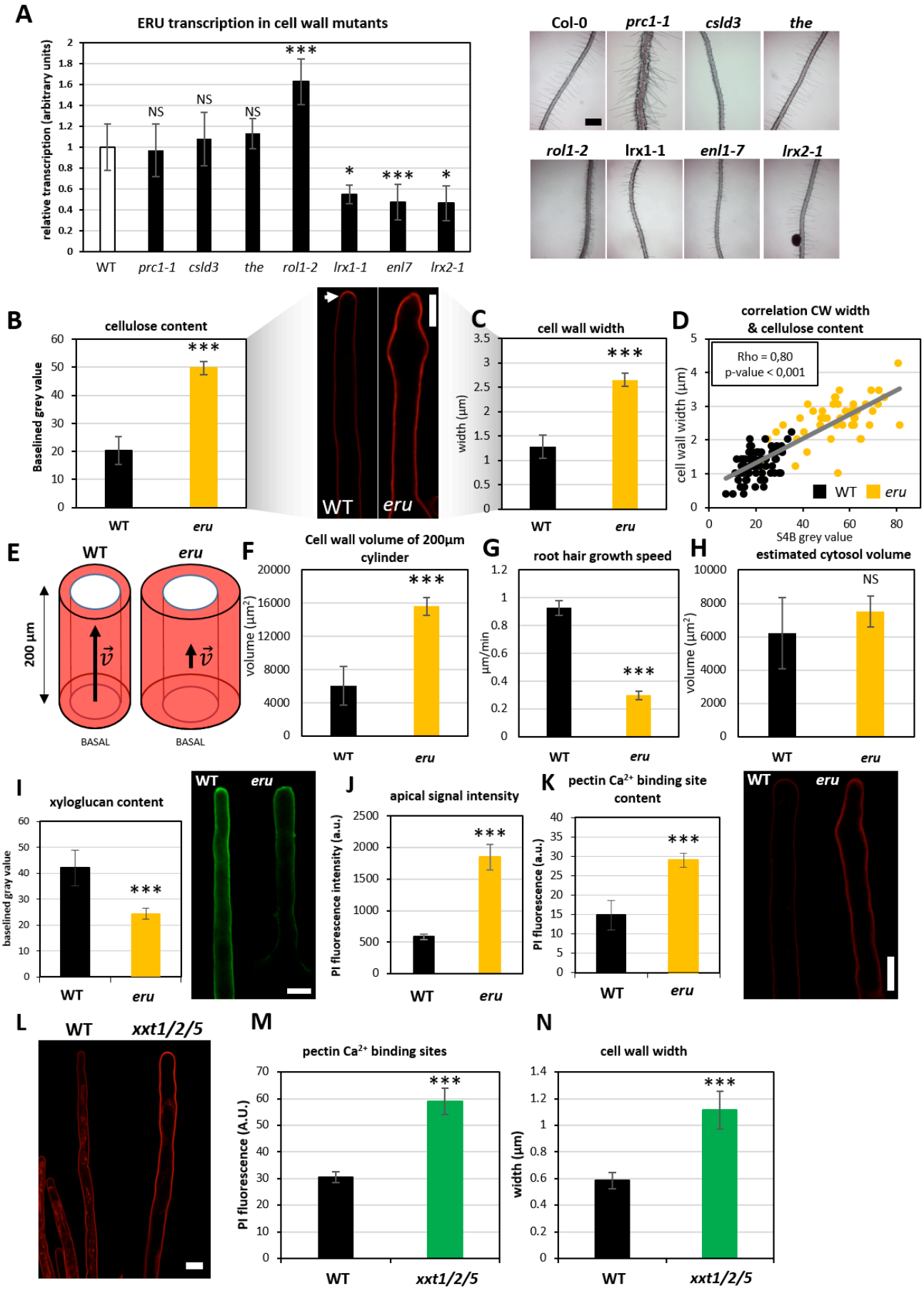
A
ERU transcription in cell wall mutants
relative transcription (arbitrary units)
WT
prc1-1
csld3
the
rol1-2
lrx1-1
enl7
lrx2-1
Col-0
prc1-1
csld3
the
rol1-2
lrx1-1
enl1-7
lrx2-1
B
cellulose content
Baselined grey value
C
cell wall width
width (µm)
D
correlation CW width & cellulose content
Rho = 0,80
p-value < 0,001
cell wall width (µm)
S4B grey value
E
WT
eru
200 µm
BASAL
F
Cell wall volume of 200µm cylinder
volume (µm²)
G
root hair growth speed
µm/min
H
estimated cytosol volume
volume (µm²)
I
xyloglucan content
baselined gray value
J
apical signal intensity
PI fluorescence intensity (a.u.)
K
pectin Ca²⁺ binding site content
PI fluorescence (a.u.)
L
xxt1/2/5
M
pectin Ca²⁺ binding sites
PI fluorescence (A.U.)
N
cell wall width
width (µm)

Figure S7. *ERU* transcription in CW mutants, *eru* CW defects and the effect of xyloglucan (XYG) deficiency on pectin composition, Related to Figure 5.

(A) *ERU* transcription is affected in specific RH mutants. qPCR data showing the transcription of *ERU* in the roots of WT (Col-0) and several CW RH mutants (n=3). Images of mature RHs of the lines used. Scale bar = 400 µm. (B-K) *Eru* RH CWs are affected in cellulose, XYG and pectin. WT and *eru* RHs were stained with direct red 23. (B) cellulose content and images of WT and *eru* RHs. The arrow shows higher cellulose deposition at the tip. Scale bar, 20 µm. (C) CW width as extracted from S4B cross-sectional intensity plots. (D) Correlation of the CW width and cellulose content revealing a positive correlation (Rho=0.80; $p<0.001$). (E) Virtual 200 µm section of the RH stalk. CW and cytoplasm volume calculated from the S4B staining. $\vec{v}$ = growth speed vector. (F) The CW volume is inversely related with (G) the RH growth speed. (H) The cytosol volume is unaffected (n=8). (I) The XYG content is reduced in *eru* RH CWs. Lm25 signal intensity (n=10 roots with > 5 RH per root). Confocal images of lm25-stained RHs. Scale bar, 20 µm. (J-K) PI staining of pectin Ca^{2+} egg-boxes. (J) average PI fluorescence intensity at the tip of growing WT and *eru* RHs. (K) average PI fluorescence intensity in the stalk of WT and *eru* RHs (n=6). representative confocal images of WT and *eru* RHs stained with PI. Scale bar, 20 µm. (L) PI stained WT and *xxt1/2/5* RHs. Scale bar, 10 µm. (M) pectin Ca^{2+} binding site abundance. (N) CW width from PI stained RHs. Error bars represent SE. Multiple RHs were measured for at least 6 roots per genotype. Significance codes p-value: 0.05 '*' 0.01 '**' <0.001 '***'.

experiment	Oligo sequence 5' to 3'	Gene/region (relative to ATG +1)
ERU genotyping	ATTTTGCCGATTTCGGAAC	LBb1.3 T-DNA specific primer
	TTTATCAACGCCGTTGAAATC	at5g61350 FW
	ATTTTGTGTCGCGGTCTGTAG	at5g61350 REV
semi quantitative RT-PCR	GGTTCGAGAAATGTCACTGTTG	FW at5g61350 T-DNA spanning
	CCAATACCCGCAATAGCAAG	REV at5g61350 T-DNA spanning
	TGGTGTCATGGTTGGGATG	ACTIN 2 FW [S2]
	CACCACTGAGCACAATGTTAC	ACTIN 2 REV [S2]
	ATGCCCCAGGACATCGTGATTTCAT	EF1α FW [S3]
	TTGGCGGCACCCTTAGCTGGATCA	EF1α REV [S3]
cloning	GGGGACAAGTTTGTACAAAAAAGCAGGCTTCGCTTTGAGGTCATTTTT	At5g61350 promoter -619 to 0
	GGGGACCACTTTGTACAAGAAAGCTGGGTAATATCCGGCGAGGTTTTGA	
	GGGGACAAGTTTGTACAAAAAAGCAGGCTTAATGGGAGGAGATTTTCGTCA	At5g61350 CDS without stop codon
	GGGGACCACTTTGTACAAGAAAGCTGGGTCCGGTATTGAATGCGACGGA	
ChIP-qPCR	AGAGACAGACAAACAGTACTTTACA	At5g61350 promoter -1455 to -1332
	AGGATCGGATGGTATATGTGTATTC	
	AGCTAAACATGGCTGTCACTAA	At5g61350 promoter -475 to -353
	GTACTAAATTGGTGGGCAGTTAAAG	
	TCTCTAAGCTCTTTGGTCGCGTGT	Control oligos: pTUB4 (At5g44340)
	TCTTCCTCTTCCGCCTCCAACTTT	
	CACAATGTTTGGCGGGATTGGTGA	Control oligos: Actin12 (At3g46520)
	TGTACTTCCTTTCCGGTGGAGCAA	
realtime PCR	TTCCGCAGACAACAACTC	At5g61350 FW
	CTCTAGGTAACTGTGGGTTTATC	at5g61350 REV
	AGGTGACTACGAGGATGAGGAAGA	TUB3 FW
	CTGCAACTGGTAGTTGAGGTTCTC	TUB3 REV

Table S1: Overview of the primers that were used for genotyping, RT-PCR, cloning, ChIP-qPCR and realtime PCR, Related to STAR Methods.

Supplemental References

S1. Winter, D., Vinegar, B., Nahal, H., Ammar, R., Wilson, G., and Provart, N. (2007). An "electronic fluorescent pictograph" browser for exploring and analyzing large-scale biological data sets. PLoS One *2*, e718.

S2. Kusano, H., Testerink, C., Vermeer, J.E.M., Tsuge, T., Shimada, H., Oka, A., Munnik, T., and Aoyama, T. (2008). The *Arabidopsis* Phosphatidylinositol Phosphate 5-Kinase PIP5K3 is a key regulator of root hair tip growth. Plant Cell *20*, 367–380.

S3. Nesi, N., Debeaujon, I., Jond, C., Pelletier, G., Caboche, M., and Lepiniec, L. (2000). The *TT8* gene encodes a basic helix-loop-helix domain protein required for expression of *DFR* and *BAN* genes in *Arabidopsis* siliques. Plant Cell *12*, 1863–1878.